

# Molecular mechanism of A $\beta$ alloform co-aggregation

Alexander J. Dear,<sup>1,2,3</sup> Georg Meisl,<sup>4</sup> Emil Axell,<sup>1</sup> Sara Linse,<sup>1,\*</sup> and L. Mahadevan<sup>2,†</sup>

<sup>1</sup>*Center for Molecular Protein Science, Lund University, 221 00 Lund, Sweden*

<sup>2</sup>*School of Engineering and Applied Sciences, Harvard University, USA*

<sup>3</sup>*Department of Biology, Institute of Biochemistry,*

*ETH Zurich, Otto Stern Weg 3, 8093 Zurich, Switzerland<sup>‡</sup>*

<sup>4</sup>*Centre for Misfolding Diseases, Department of Chemistry,  
University of Cambridge, Lensfield Road, Cambridge CB2 1EW, United Kingdom*

(Dated: January 31, 2025)

Analyzing kinetic experiments on protein aggregation using integrated rate laws has led to numerous advances in our understanding of the fundamental chemical mechanisms behind amyloidogenic disorders such as Alzheimer’s and Parkinson’s diseases. However, biologically relevant processes may be governed by rate equations that are too complex to solve using existing methods, hindering mechanistic insights into these processes. An example of significance is co-aggregation in environments containing multiple A $\beta$  peptide alloforms, which may play a crucial role in the biochemistry of Alzheimer’s disease but whose mechanism is still poorly understood. Here, we develop using the mathematics of symmetry a highly general integrated rate law valid for most plausible linear self-assembly reactions. We use it in conjunction with experimental data to determine the mechanism of co-aggregation of A $\beta$ 42, A $\beta$ 40, A $\beta$ 38 and A $\beta$ 37 peptides. We find that A $\beta$ 42 fibril surfaces enable the formation of co-oligomers, which accelerate new A $\beta$ 40, A $\beta$ 38 and A $\beta$ 37 fibril formation whilst inhibiting secondary nucleation of new A $\beta$ 42 fibrils. The simplicity, accuracy and broad applicability of our general solution will encourage its widespread adoption by researchers modelling filamentous self-assembly kinetics, both with and without co-aggregation.

## I. INTRODUCTION

The self-assembly of proteins and peptides into amyloid fibrils has been intensively studied in the past decades due to its key role in a multitude of increasingly prevalent and incurable human pathologies, such as type-II diabetes, Alzheimer’s and Parkinson’s diseases [1, 2]. The kinetics of the self-assembly process have been found to be well-described by differential equations that, although relatively simple, do not normally possess exact analytic solutions. Instead, great success has been had in developing accurate approximate analytic solutions for several particularly important mechanisms of self-assembly [3–9]. These expressions have been widely fitted to experimental data in order to identify the constituent reaction steps and their associated rate constants for many different proteins under diverse conditions [10]. This has enabled fundamental discoveries about the chemical mechanisms behind the formation of both pathological and functional amyloid [11], ranging from Amyloid- $\beta$  and tau fibrils in Alzheimer’s disease [6, 9, 12, 13] to functional yeast prions in *S. cerevisiae* [14] and bacterial biofilms [15]. Such solutions are also used in the screening of candidate inhibitory drugs for the treatment of aggregation-related diseases [16–18].

Now that many of the fundamental aggregation reactions have been characterized, researchers have become increasingly interested in less idealized and more realis-

tic representations of the self-assembly process, described by more complex kinetic equations. In particular, interactions between different proteins or different forms of a protein during aggregation *in vivo* is expected to be the norm rather than the exception, given that biological environments tend to contain multiple self-assembly-prone species as well as other molecular factors in close proximity. For instance, post-translational modifications appear to play an important role during *in vivo* aggregation of tau [19], and the co-aggregation of lipids and protein likely plays an important role in  $\alpha$ -synuclein aggregation [20]. Another particularly notable example is the large number of different length-variants (alloforms) and post-translationally modified variants of the Alzheimer’s disease-associated A $\beta$  peptide [21, 22] that appear to be involved in aggregate formation during the disease. Several of these variants occur *in vivo* at non-negligible concentrations, and have been shown or proposed to have differing effects on both the aggregation rate and the progression of the disease [21–28]. A complete understanding of Alzheimer’s disease will likely require a full understanding of the ways in which these proteins interact during aggregation into fibrils. Some such co-aggregation reactions have already been studied experimentally *in vitro* [25, 29–34]. However, the most popular technique for deriving analytical solutions for simpler systems, fixed-point theory [3–6], is applicable to multi-component self-assembly reactions only under very specific circumstances [35]. These circumstances do not apply to the co-aggregation of A $\beta$  variants, limiting the kinetic analysis that could be performed at the time.

In recent work [36], we posited that the theory of approximate Lie groups, when appropriately extended,

\* sara.linse@biochemistry.lu.se

† lm@seas.harvard.edu

‡ alexander.dear@bc.biol.ethz.ch

might provide a unifying theoretical basis to a wide range of singular perturbation techniques, including but not limited to the method of multiple scales, and the perturbative renormalization group of Chen, Oono and Goldensfeld (CGO RG). This hypothesis was inspired by the little-known fact that most techniques for the exact solution of differential equations (DEs) rely implicitly on the identification and exploitation of exact continuous (Lie) symmetries [37]. This raises the questions: can protein aggregation kinetics be treated in a unified way by Lie symmetry methods, can these be used to solve the kinetics of co-aggregation of A $\beta$  variants, and what could such solutions teach us about the mechanism of their co-aggregation?

In the Methods we present a general solution for the kinetics of a very broad class of protein aggregation reactions, formulated in terms of series solutions of differential equations. Although its validity rests on the mathematics of Lie symmetry, we relegate to the Supporting Information (SI) its full Lie theoretic derivation. We do so since, although powerful and elegant, Lie theoretic techniques for differential equations are highly specialized and not widely known.

In the Results we first determine the rate equations describing the co-aggregation of the key A $\beta$  alloforms A $\beta$ 42, A $\beta$ 40, A $\beta$ 38 and A $\beta$ 37. We then present the solutions using our new method to these equations; mathematically interested readers can find the corresponding derivations in SI Sec. S2. (To aid the reader we also provide a reference table of mathematical notation in SI Sec. S9.) To determine what these solutions teach us about the mechanism of co-aggregation, we use both new and published experimental data on A $\beta$ 42, A $\beta$ 40, A $\beta$ 38 and A $\beta$ 37 co-aggregation to identify the molecular mechanisms by which A $\beta$ 40, A $\beta$ 38 and A $\beta$ 37 inhibit A $\beta$ 42 aggregation, and by which A $\beta$ 42 promotes A $\beta$ 40 and A $\beta$ 38 aggregation. We next show how both of these effects are consequences of the same fundamental phenomenon. In the Discussion we conclude by exploring the implications both of our findings about A $\beta$  co-aggregation and of our new method.

## II. METHODS

Sec. II A introduces terminology and general rate equations that describe a wide range of protein aggregation reactions, and also introduces dimensionless parameters. In Sec. II B we develop a perturbative expansion of these rate equations and explain why most standard approximate methods fail to produce a viable solution. In Sec. II C we describe qualitatively our new method in a way that does not require knowledge of Lie symmetries or group theory, and present a general solution to the rate equations. Finally, Secs. II D-II E outline the experimental techniques used to collect new co-aggregation data, and how these data are subsequently processed.

### A. Highly generalized rate equations for protein fibril formation reactions

The kinetics of amyloid fibril self-assembly in a closed *in vitro* system can generally be modelled by developing rate equations for the fibril number concentration  $P(t)$ , fibril mass concentration  $M(t)$ , and the monomer concentration  $m(t)$ . Since amyloid fibrils typically contain a small number of monomers per plane, but a very large number of planes per fibril, their aggregation can be accurately modelled as a linear self-assembly reaction.

New protein fibrils form from monomer in solution through a slow primary nucleation reaction step (often mediated by third-party interfaces such as the air-water interface or plate walls [9, 38, 39], and subsequently elongate rapidly by monomer addition (Fig. 1a). Elongation does not create or remove fibrils and thus only affects  $M(t)$  and  $m(t)$  (decreasing the latter with rate proportional to  $m(t)P(t)$ ). Since nucleation is much slower than elongation, the monomer lost during nucleation can be ignored and to a good approximation primary nucleation increases only  $P(t)$  (with rate dependent only on monomer concentration). Most amyloid-forming systems also feature reaction steps whose rates are proportional to the fibril mass concentration  $M(t) = m_{\text{tot}} - m(t)$ , sometimes summarised as multiplication processes or secondary processes. Such processes induce autocatalytic amplification in filamentous self-assembly. They include fibril fragmentation (rate  $k_-M(t)$ ) as well as secondary nucleation of new fibrils on the surface of existing fibrils (Fig. 1a; rate dependent on both  $m(t)$  and  $M(t)$ ).

The simplest rate laws possible for a closed chemical system containing all three processes are:

$$\frac{dP}{dt} = k_n m(t)^{n_c} + k_2 m(t)^{n_2} M(t) \quad (1a)$$

$$\frac{dM}{dt} = 2k_+ m(t)P(t), \quad m_{\text{tot}} = M(t) + m(t), \quad (1b)$$

where  $k_n$ ,  $k_2$  and  $k_+$  are by convention the rate constants of primary and secondary nucleation and of elongation respectively, and  $n_c$  and  $n_2$  the reaction orders for the nucleation processes. Fragmentation can be described by the same equations by setting  $n_2 = 0$  and  $k_2 = k_-$ . The final equation is the closure relation ( $m_{\text{tot}}$  is the total (constant) concentration of protein molecules in monomers and fibrils). These equations will be familiar to researchers who have previous knowledge of amyloid formation kinetics.

We wish to be as general as possible about amyloid kinetics in this paper, so we consider a much more general form for the kinetic equations that can capture a range of more complex behaviours such as co-aggregation, multi-step nucleation and enzyme-like saturation effects. This can be done by writing them in the form:

$$\frac{dP}{dt} = \alpha_1(t, m) + \alpha_2(m)M(t) \quad (2a)$$

$$\frac{dM}{dt} = \alpha_e(m)P(t), \quad m_{\text{tot}} = M(t) + m(t). \quad (2b)$$

Here,  $\alpha_1(t, m)$  is a general rate law for primary nucleation processes, depending on time  $t$  both explicitly and implicitly via  $m(t)$ . Only in the simplest possible case does it equal  $k_n m(t)^{n_c}$  (having no explicit  $t$ -dependence in this case). Similarly,  $\alpha_2 M$  and  $\alpha_e P$  are general expressions for the rates of secondary processes and of elongation; since elongation is monomer-dependent,  $\lim_{m \rightarrow m_c} \alpha_e = 2k_+(m - m_c)$ , where  $m_c$  is the monomer solubility. For aggregation reactions (i.e. starting with an excess of monomer),  $\alpha_1$ ,  $\alpha_e$  and  $\alpha_2$  are always  $> 0$ .

Certain restrictions on the forms of these rates are necessary for the applicability of the Lie symmetry method we develop. First,  $\alpha_1(t, m)$  must be smaller than  $\alpha_2$  when  $t = 0$  and  $\alpha_1(t, m_{\text{tot}})$  must grow less rapidly with  $t$  than  $e^{\kappa t}$ , where  $\kappa = \sqrt{\alpha_e(m_{\text{tot}})\alpha_2(m_{\text{tot}})}$ . As will be seen later, this restriction holds for all reactions where secondary processes are important. Second,  $\alpha_2$  and  $\alpha_e$  must depend on constant parameters  $\mathbf{d}$  in such a way that  $\mathbf{d} = 0$  reduces them to  $\alpha_2(m, \mathbf{d} = 0) = k_2 m^{n_2}$ , and  $\alpha_e(m, \mathbf{d} = 0) = 2k_+ m$ . Many possible rate laws for elongation and secondary processes can be written in this way. For example, saturated elongation can be captured by this formalism with  $\alpha_e = 2k_+ m(t)/(1 + m(t)/K_E)$  [9]. Indeed, excepting those that explicitly model nonfibrillar oligomers, almost all previously discovered rate laws describing amyloid fibril formation are captured by these forms. Crucially, this restriction ensures that Eqs. (2) admit a special analytical solution (Eq. (S27); derived in SI Sec. S2B) when  $\mathbf{d} = \alpha_1(0, m_{\text{tot}}) = 0$  and  $P(0)$  is a particular function of  $M(0)$ . Although not useful in itself, its existence will later enable us to solve these equations generally.

## B. Divergent perturbative expansions for the rate equations

An important first step for mathematical analysis of equations in general is to nondimensionalize them to remove their units. This often simplifies their structure and reduces the number of constants they depend on [40]. Defining  $\mu = m(t)/m_{\text{tot}}$  and  $\kappa = \sqrt{\alpha_e(m_{\text{tot}})\alpha_2(m_{\text{tot}})}$ , we can productively nondimensionalize and simplify Eqs. (2) using  $\tau = \kappa t$  and  $\Pi(\tau) = \alpha_e(m_{\text{tot}})P(t)/m_{\text{tot}}\kappa$ , yielding:

$$\frac{d\Pi}{d\tau} = 2\varepsilon \frac{\alpha_1(t, m)}{\alpha_1(0, m_{\text{tot}})} + \frac{\alpha_2(m)}{\alpha_2(m_{\text{tot}})}(1 - \mu(\tau)) \quad (3a)$$

$$\frac{d\mu}{d\tau} = -\frac{\alpha_e(m)}{\alpha_e(m_{\text{tot}})}\Pi(\tau), \quad (3b)$$

where  $\varepsilon = \alpha_1(0, m_{\text{tot}})/2m_{\text{tot}}\alpha_2(m_{\text{tot}})$ , which can be interpreted as the relative importance of primary nucleation over secondary processes.

By definition,  $1 \geq \mu(0)$  and  $\Pi(0) \geq 0$ . Moreover, in aggregation reactions  $\alpha_1$ ,  $\alpha_2$  and  $\alpha_e$  are never negative. Consequently,  $\Pi$  is monotonic increasing, and  $\mu$  is monotonic decreasing. The structure of the parameter

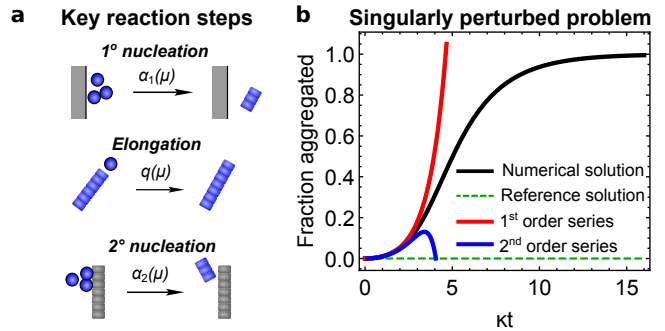


FIG. 1. Demonstration that the perturbative solution of Eqs. (3) is divergent (illustrated for  $\mathbf{d} = 0$  and  $\alpha_1$  with no explicit time dependence). **a**: Key reaction steps involved. **b**: Parameters:  $n_2 = 3$ ,  $n_c = 2$ ,  $\varepsilon = 0.01$ ,  $\Pi(0) = 0$ ,  $\mu(0) = 1$ , and  $\alpha_1 = \alpha_2 = \alpha_e = \text{const}$ . After a short initial time period the first- and second-order perturbation series (Eq. (6a), red and Eq. (S40), blue) diverge away from the exact numerical solution to Eqs. (3), black.

space relevant to protein aggregation is therefore simple, featuring only an attractive fixed point at  $\mu = m_c$ . If we make the approximation of irreversibility,  $m_c = 0$  and the parameter space can be partitioned into two parts: the  $\mu \rightarrow 0$  asymptotic region, characterized by linearized kinetics about the fixed point, and the remainder, the  $\mu \rightarrow 1$  asymptotic region. For small  $\varepsilon$  the kinetics approximately linearize when  $\alpha_2(m_{\text{tot}}\mu)/\alpha_2(m_{\text{tot}}) \rightarrow 0$  and when  $\alpha_e(m_{\text{tot}}\mu)/\alpha_e(m_{\text{tot}})$  becomes linear in  $\mu$ . The  $\mu \rightarrow 0$  asymptotic region thus corresponds to the kinetics becoming dominated by single-step elongation of fibrils, with nucleation no longer being important. The  $\mu$  value at which this occurs represents the boundary between these two asymptotic regimes. Often, the dynamics within the  $\mu \rightarrow 1$  region are uniform and no meaningful further subdivision of the parameter space exists, in which case the special singular perturbation series that we will derive below remains accurate throughout this region.

Eqs. (3) cannot be solved exactly for  $M(t)$ , similarly to the less general Eqs. (1) [3, 4]. Nonetheless, since analytical solutions possess a number of advantages over numerical integration, accurate approximate solutions to these equations are of great value. Indeed, the greater clarity and simplicity can often make simple approximate solutions even more useful than exact solutions. Many techniques for obtaining globally valid approximate solutions to differential equations use perturbation theory as a starting point. This amounts to looking for a series solution in a (usually small) parameter  $s$  entering the equations. For general differential equation  $F(y, x, s, dy/dx, d^2y/dx^2, \dots) = 0$ , we would first make the substitution  $y(x) = \sum_{i=0} s^i y^{(i)}(x)$  and then collect terms in powers of  $s$ . The equations at each order in  $s$  are often simpler than the original equation, permitting  $y^{(0)}$ ,  $y^{(1)}$ , etc to be sequentially calculated. Even just the first two or three terms of this series can give an accurate

approximate solution.

Writing the initial conditions as  $\{\mu(0) = 1 - \delta, \Pi(0) = p\}$ , Eqs. (3) admit a perturbation series in  $\varepsilon$ ,  $\delta$  and  $p$ . To simplify the perturbation calculations, we first replace these with  $s\varepsilon$ ,  $s\delta$  and  $sp$ , where  $s$  is a bookkeeping parameter to be later set to 1. We then expand Eqs. (3) in  $s$ , resulting in the following perturbation equations. At  $O(s^0)$ :

$$\frac{d\Pi^{(0)}}{d\tau} = \frac{\alpha_2(m_{\text{tot}}\mu^{(0)})}{\alpha_2(m_{\text{tot}})}(1 - \mu^{(0)}), \quad \Pi^{(0)}(0) = 0, \quad (4a)$$

$$\frac{d\mu^{(0)}}{d\tau} = -\frac{\alpha_e(m_{\text{tot}}\mu^{(0)})}{\alpha_e(m_{\text{tot}})}\Pi^{(0)}, \quad \mu^{(0)}(0) = 1. \quad (4b)$$

These can be solved by  $\mu^{(0)}(\tau) = 1$ ,  $\Pi^{(0)}(\tau) = 0$ . The  $O(s^1)$  equations are:

$$\frac{d\Pi^{(1)}}{d\tau} = 2\varepsilon \frac{\alpha_1(t, m_{\text{tot}})}{\alpha_1(0, m_{\text{tot}})} - \mu^{(1)}, \quad \Pi^{(1)}(0) = p \quad (5a)$$

$$\frac{d\mu^{(1)}}{d\tau} = -\Pi^{(1)}, \quad \mu^{(1)}(0) = -\delta. \quad (5b)$$

Provided  $\alpha_1(t, m_{\text{tot}})$  is integrable, this is solved by:

$$\mu^{(1)}(\tau) = -\left[\varepsilon\mathcal{F}(\tau) + \frac{\delta}{2}(e^\tau + e^{-\tau}) + \frac{p}{2}(e^\tau - e^{-\tau})\right] \quad (6a)$$

$$\Pi^{(1)}(\tau) = \varepsilon\dot{\mathcal{F}}(\tau) + \frac{\delta}{2}(e^\tau - e^{-\tau}) + \frac{p}{2}(e^\tau + e^{-\tau}), \quad (6b)$$

where  $\mathcal{F}(\tau)$  satisfies  $\mathcal{F}(0) = \dot{\mathcal{F}}(0) = 0$  and  $\lim_{\tau \rightarrow \infty} \mathcal{F}(\tau)e^{-\tau} = c_\varepsilon$ , with  $c_\varepsilon$  a positive constant. In the common case that  $\alpha_1$  has no explicit time-dependence,  $\mathcal{F}(\tau) = e^\tau + e^{-\tau} - 2$ .

Very often, perturbation series for nonlinear differential equations actually only provide accurate solutions near where the initial or boundary conditions have been imposed. They are said to be singular, and diverge from the true solution away from the initial or boundary conditions.  $\sum_i s^i \mu^{(i)}$  is an example of such singular perturbation series, being valid only *asymptotically* towards the phase point corresponding to the initial conditions (Fig. 1b). Unusually, however, whereas a typical singular perturbation series can be solved for arbitrary initial or boundary conditions, permitting this phase point to be moved arbitrarily, the region of validity of this series is instead fixed around  $\{\mu(0) = 1, \Pi(0) = 0\}$ , since these are the only initial conditions for which it solves Eqs. (4)-(5). We refer to such singular perturbation series, in which the initial or boundary conditions contain perturbation parameters, as “local perturbation series”.<sup>1</sup>

Standard singular perturbation series can often be converted into globally valid solutions using so-called “singular perturbation methods”. In a recent work [36] we demonstrated that the mathematical basis of many of the most popular and powerful singular perturbation methods, including Chen-Goldenfeld-Oono Renormalization Group, the Method of Multiple Scales, and reductive perturbation, originates in certain symmetry properties of the differential equation’s solution. At this stage we do not need to know the nature of these symmetry properties. The key relevant finding is that these techniques are valid only when these symmetry properties are inherited by the solution’s singular perturbation series, which occurs only if the series contains undetermined constants of integration. Consequently, such methods cannot be used here, since local perturbation series cannot be solved for arbitrary initial or boundary conditions. As discussed above, an unusual singular perturbation technique called fixed-point theory has been successfully employed when  $\alpha_1$ ,  $\alpha_2$  and  $\alpha_e$  are sufficiently simple [3–6]. However, for more complex protein aggregation reactions such as those involving co-aggregation or inhibition it is usually inapplicable, necessitating development of a new method.

### C. General solution to the rate equations using Lie symmetries

The basic idea of the method is to symmetry-transform a known *special* solution to Eqs. (3), valid for *specific* choices of the constant parameters entering the equations and their initial conditions, into a *general* solution valid for *any* parameter values. As stated above, such a solution (Eq. (S27)) is available for Eqs. (2) (or equivalently Eqs. (3)). The procedure for transforming this special solution into a general one can be derived from Lie group theory by considering a type of symmetry called an “asymptotic symmetry”. It is fundamentally different from the class of symmetries underlying the most popular singular perturbation techniques mentioned above, which are instead known as “approximate Lie symmetries” [36, 42].

Using this method, the general solution to protein aggregation rate equations of the form Eq. (2) is:

$$M(t) = m_{\text{tot}} - m_{\text{tot}} \left(1 - \frac{\mu^{(1)}(\kappa t)}{c_1}\right)^{-c_1} \quad (7a)$$

$$\kappa = \sqrt{\alpha_e(m_{\text{tot}})\alpha_2(m_{\text{tot}})} \quad (7b)$$

$$c_1 = \frac{3}{2n'_2 + 1}, \quad n'_2 = \frac{d \ln [\alpha_2(m)\alpha_e(m)^2]}{d \ln m} \Big|_{m=m_{\text{tot}}} - 2, \quad (7c)$$

and  $\mu^{(1)}$  is the solution Eq. (6a) to the first order perturbation equation Eq. (5). Since the study of asymptotic symmetries is a very obscure sub-field of Lie group theory, we relegate the method itself and its derivation to SI Sec. S2.

<sup>1</sup> Note that a local perturbation series is not the same as a perturbation series in the independent variables, which is usually referred to as local analysis [41].

There is one further condition that needs to be met for the applicability of our method, and therefore the validity of Eq. (7), beyond the aforementioned restrictions on the rate terms entering Eq. (2). In technical terms, this condition is that the asymptotic symmetry underlying the method is approximately valid globally in the parameter space of interest (see SI for a technical explanation). In practical terms, this means that Eq. (7) is only applicable to aggregation reactions that fall into one of two general classes. These can be expressed without discussing Lie symmetries as follows. First, if the parameters that are set to zero in the special solution drop out of the  $\mu \rightarrow 0$  kinetics at leading order. Most unsaturated single-protein aggregation reactions with low or no seeding fall into this class (see SI Sec. S5C). The second class is kinetic equations for which the boundary between asymptotic regions is sufficiently close to  $\mu = 0$  that the  $\mu \rightarrow 0$  region has negligible extent. Most reactions featuring saturation of secondary nucleation, including the co-aggregation reactions studied here, fall into this second class. Unsaturated, highly seeded aggregation reactions (where  $M(0)/m_{\text{tot}}$  or  $\alpha_e(m_{\text{tot}})P(0)/m_{\text{tot}}\kappa$  are not small) or reactions with slow secondary processes (i.e.  $\varepsilon$  is not small) fall into neither class; its treatment by asymptotic symmetry methods requires an extension of the methodology to be explored in a future paper.

## D. Experimental methods

### 1. Chemicals and consumables

Unless otherwise specified, the experimental buffer used was always 20 mM sodium phosphate, 0.2 mM EDTA at pH 7.4. The buffers used were always filtered through wwPTFE (0.22  $\mu\text{m}$ , 60539, Pall corporation) and degassed prior to use. Thioflavin T (ThT) was purchased from CalBiochem.

### 2. Expression & purification of A $\beta$ variants

The sequences for A $\beta$ (M1-42), A $\beta$ (M1-40), A $\beta$ (M1-38) and A $\beta$ (M1-37) referred to in this work as A $\beta$ 42, A $\beta$ 40, A $\beta$ 38 and A $\beta$ 37 were prepared using overlapping PCR and cloned in PetSac plasmid as reported in [43] and [34], see [44] for detailed protocol. In brief, the peptides were expressed in *Escherichia coli*, strain BL21 Star (DE3) pLysS for A $\beta$ 42 and A $\beta$ (M1-37), BL21-Gold (DE3) pLysS (Invitrogen, Waltham, MA, USA) for A $\beta$ 38 and T7 Express (New England Biolabs, Ipswich, MA, USA) was used for A $\beta$ (M1-40). After harvesting and lysis of the cells, the peptide was isolated from inclusion bodies through a series of ion-exchange chromatography steps [44]. Aliquots of the purified proteins were lyophilised and kept frozen until further use.

### 3. Isolation of monomers

Prior to each kinetic experiment, a freeze-dried peptide aliquot was reconstituted in 1 mL 6M guanidine hydrochloride and subjected to separation on a 10/300 Superdex 75 increase, size exclusion column. This was done to ensure the highest possible degree of homogenous monomer at the start of each experiment. The monomers were isolated in the desired experimental buffer and their concentration was determined by integration of the chromatogram monitored at 280 nm and calculated using Beers-law, using an extinction coefficient of 1490  $\text{M}^{-1}\text{cm}^{-1}$

### 4. Aggregation kinetics

Aggregation kinetics were followed by monitoring the increase of fibril mass through the fluorescent signal of 5  $\mu\text{M}$  ThT at excitation 448 nm and emission 480 nm. The reactions were performed with 100  $\mu\text{L}$  in each well (3881, Corning, USA) in a FLUOstar Omega (BMG LABTECH).

## E. Data processing

The data displayed in Fig. 7A of ref. [30] exhibits relatively high variability between replicates in the half-time of the second sigmoid, corresponding to A $\beta$ 40 aggregation. Plotting all replicates visually obscures the trend in half time versus A $\beta$ 42 seed concentration for this transition. Some of this variability originates from variability in ThT fluorescence, as evident from the large spread in values for the first ThT plateau's relative height. Since the direction of this trend is important in determining the mechanism of co-aggregation, we performed some additional data processing steps prior to re-plotting these curves and fitting our kinetic models to them.

First, each curve was divided into two time portions, each containing one of the two sigmoids. This allowed us to normalize each sigmoid independently, and to remove certain large jumps or discontinuities between adjacent time points that were clearly artefactual. The two portions were then recombined with appropriate normalization factors to ensure that the recombined curves reflect relative fibril mass concentration. This processing step already reduced the variability in the half time for the second sigmoid, although still larger than desired.

As a second step, we retained only the replicates with the median second-sigmoid half time for each condition. For conditions with even numbers of replicates, we averaged over the two curves with median half-times. The resulting curves, displayed in Fig. 4a-b, are much more easily interpretable than the raw data displayed in ref. [30]. Note, comparatively very little variability was evident in the half-times of the first sigmoid prior to removing these replicates.

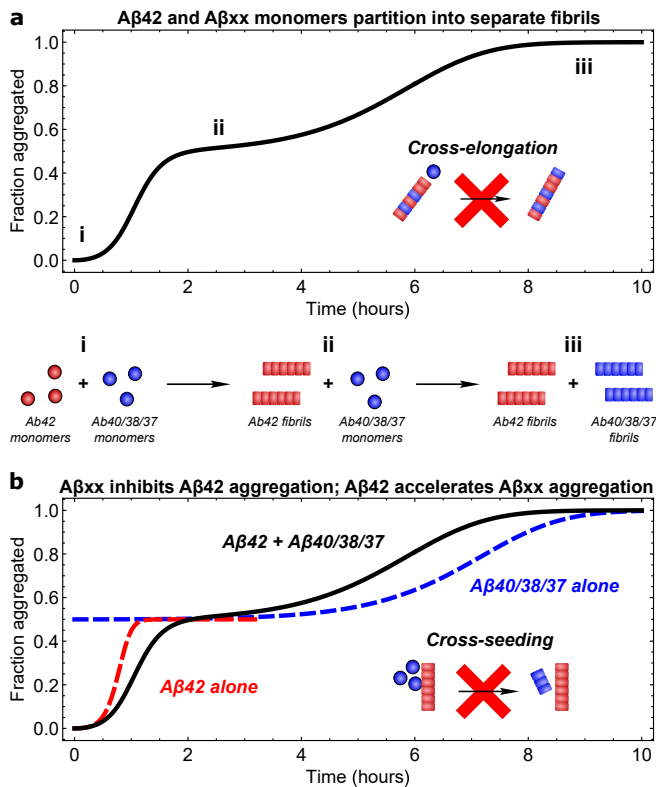


FIG. 2. Schematic of A $\beta$ 42 co-aggregation with A $\beta$ 40/38/37 (A $\beta$ xx). **a**: A $\beta$ 42 and A $\beta$ xx co-aggregation at pH 7.4 shows separate sigmoidal increases in fibril mass, with the first corresponding to pure A $\beta$ 42 fibril formation, and the second to pure A $\beta$ xx fibril formation. Thus, no significant cross-elongation occurs. **b**: Monomeric A $\beta$ xx has a clear inhibitory effect on A $\beta$ 42 fibril formation, whereas monomeric A $\beta$ 42 accelerates A $\beta$ xx fibril formation. (Addition of pure A $\beta$ 42 fibrils to monomeric A $\beta$ xx was found in refs. [30, 34] not to accelerate or “cross-seed” nucleation of new A $\beta$ xx fibrils.) The detailed mechanism of these inhibitory and accelerating effects was heretofore unknown and is a key focus of the present study.

We performed identical data processing methodology for the kinetic curves measured in the fresh experiments we performed ourselves as part of this study. These are displayed in Fig. 4c-d.

### III. RESULTS

#### A. Rate laws for A $\beta$ alloform co-aggregation

In recent studies the co-aggregation of A $\beta$ 40, A $\beta$ 37 or A $\beta$ 38 (hereafter referred to collectively as A $\beta$ xx) with A $\beta$ 42 under physiologically relevant conditions (in 20 mM sodium phosphate and 0.2 mM EDTA at pH 7.4, without agitation) has been monitored over time by Thioflavin T (ThT), a dye that fluoresces when it binds to amyloid fibrils. The resultant kinetic curves describing the transformation of monomeric to fibrillar protein feature two

separate sigmoidal transitions (Fig. 2a). Using separate stable isotopes in A $\beta$ 40 and A $\beta$ 42, and identification using mass spectrometry [30], as well as analytical high performance liquid chromatography [34], the first transition was established to correspond to the formation of fibrillar A $\beta$ 42, and the second to the formation of fibrils consisting exclusively of A $\beta$ xx, implying no cross-elongation reaction steps occur.

Since the second sigmoid occurs earlier than that observed during the aggregation of its associated shorter peptide in isolation, nucleation of new A $\beta$ xx fibrils must nonetheless be accelerated by monomeric A $\beta$ 42, aggregated A $\beta$ 42, or the two together. Addition of pre-formed A $\beta$ 42 fibril seeds to pure A $\beta$ 40 monomers failed to catalyze aggregation of the latter [30]. Aggregation of pure A $\beta$ 37 or A $\beta$ 38 monomers was weakly catalyzed by addition of A $\beta$ 42 seeds, but less effectively than by A $\beta$ 42 monomers [34]. It was thus deduced that A $\beta$ xx nucleation is accelerated by formation of co-oligomers of A $\beta$ 42 and A $\beta$ xx. We refer to this as “co-nucleation”. It was also found that the shorter peptide in monomeric form always inhibits slightly the aggregation of A $\beta$ 42 (Fig. 2b).

However, without the ability to solve analytically the rate equations describing different candidate reaction networks, it was not possible at the time to correctly identify or confirm the mechanisms of co-nucleation and cross-inhibition of these peptides. The origin of co-oligomers was thus proposed to be “primary” co-nucleation, i.e. co-nucleation without the involvement of any fibrillar species. With the more sophisticated tools we develop here we are now able to show, by globally fitting the data, that in fact the formation of co-oligomers occurs at the surface of A $\beta$ 42 fibrils, explaining both the origin of co-oligomers and the slight inhibitory effect of A $\beta$ xx on A $\beta$ 42 aggregation.

We begin our analysis by building explicit kinetic models of A $\beta$ 42 aggregation in which the A $\beta$ xx monomer inhibits one of the reaction steps. We use the subscripts  $a$  and  $b$  to signify concentrations of species consisting of A $\beta$ 42 and A $\beta$ xx, respectively, and brackets ( $a$ ) and ( $b$ ) to denote the corresponding homomolecular rate constants. One important change from homomolecular kinetic models is that we use  $P_{a/b}$  to refer to concentrations of fibril ends rather than fibril numbers, since in principle a co-nucleation event could produce a fibril with an A $\beta$ 42 residue at one end and an A $\beta$ xx residue at the other. This modifies the expressions for the various homomolecular rates by a factor of 2, as will be seen. Since A $\beta$ xx is almost entirely unaggregated during aggregation of A $\beta$ 42 in the co-aggregation experiments we are studying (Fig. 2), its concentration  $m_b$  is well-approximated as constant at its initial value  $m_{\text{tot},b}$  when modelling the aggregation of A $\beta$ 42 monomer into fibrils. Therefore, we expect that the first sigmoid, corresponding to A $\beta$ 42 aggregation, can be

described by kinetic equations of the form:

$$\frac{dP_a}{dt} = \alpha_{1,a}(m_a) + \alpha_{2,a}(m_a)M_a, \quad (8a)$$

$$\frac{dM_a}{dt} = \alpha_{e,a}(m_a)P_a, \quad M_a + m_a = m_{\text{tot},a}, \quad (8b)$$

where  $\alpha_{1,a}$ ,  $\alpha_{e,a}$  and  $\alpha_{2,a}$  express the monomer-dependence of the rates of primary nucleation, elongation and secondary nucleation of A $\beta$ 42 fibrils.

Since the first sigmoidal transition is never accelerated by A $\beta$ xx, any co-nucleation step must produce new A $\beta$ 42 fibrils much slower than ordinary A $\beta$ 42 primary nucleation; thus, we may neglect co-nucleation in our models of A $\beta$ 42 aggregation. The dependence of the rates on  $m_{\text{tot},b}$  therefore purely reflects its inhibitory effects. Since the concentration of fibril ends and primary and secondary nucleation sites is typically low, monomer binding should obey partial or pre-equilibrium [9]. So, the inhibitory effects of A $\beta$ xx monomer on A $\beta$ 42 primary nucleation and elongation can be modelled using the perturbed rate laws of refs. [17, 45]:

$$\alpha_{1,a}(m_a) = \frac{2k_n(a)m_a^{n_c(a)}}{1 + m_{\text{tot},b}/K_P(ba)}, \quad (9a)$$

$$\alpha_{e,a}(m_a) = \frac{k_+(a)m_a}{1 + m_{\text{tot},b}/K_E(ba)}, \quad (9b)$$

where  $K_P(ba)$  and  $K_E(ba)$  are equilibrium constants for dissociation of A $\beta$ xx monomer from the catalytic sites for A $\beta$ 42 fibril primary nucleation and elongation, respectively.

Modelling inhibition of secondary nucleation is more complicated, because A $\beta$ 42 secondary nucleation is at least partly saturated under the reaction conditions (meaning that monomeric protein binds faster to the fibril surface than surface-bound monomer can convert to new fibrils [6]). The rate of inhibited secondary nucleation is found (see SI Sec. S4) to be:

$$\alpha_{2,a}(m_a) = \frac{2k_2(a)m_a^{n_2(a)}}{1 + (m_a/K_S(a))^{n_2(a)} + m_{\text{tot},b}/K_S(ba)}. \quad (10)$$

Since A $\beta$ xx fibrils form in significant quantities only long after A $\beta$ 42 monomers, any interactions between the two can be neglected. (In any case, there is evidence that such interactions, if they exist, are weak [30].) So, it is reasonable to model the aggregation of A $\beta$ xx monomers into fibrils as follows:

$$\frac{dP_b}{dt} = \alpha_{1,b}(m_a, m_b) + \frac{2k_2(b)m_b^{n_2(b)}}{1 + (m_b/K_S(b))^{n_2(b)}}M_b \quad (11a)$$

$$\frac{dM_b}{dt} = k_+(b)m_bP_b, \quad (11b)$$

$$\alpha_{1,b}(m_a, m_b) = \alpha_{1,bb}(m_b) + \alpha_{1,ba}(m_a, m_b) + \alpha_{2,ba}(m_a, m_b)M_a, \quad (11c)$$

where we have replaced  $\alpha_{2,b}$  and  $\alpha_{e,b}$  with the known rate laws [6, 34] for A $\beta$ 40 and A $\beta$ 38 elongation and secondary nucleation. The total A $\beta$ xx primary nucleation rate  $\alpha_{1,b}$  contains contributions from the rates of production of new A $\beta$ xx fibril ends via primary co-nucleation and secondary co-nucleation on A $\beta$ 42 fibrils,  $\alpha_{1,ba}$  and  $\alpha_{2,ba}$  respectively, as well as the rate of normal A $\beta$ xx primary nucleation  $\alpha_{1,bb}$ . These rates are:

$$\alpha_{1,bb}(m_b) = 2k_n(b)m_b^{n_c(b)} \quad (12a)$$

$$\alpha_{1,ba}(m_a, m_b) = 2k_n(ba)m_a^{n_c(ba)}m_b^{n_c(bb)} \quad (12b)$$

$$\alpha_{2,ba}(m_a, m_b)M_a = 2k_2(ba)m_a^{n_2(ba)}m_b^{n_2(bb)}M_a. \quad (12c)$$

## B. A $\beta$ 40 and A $\beta$ 38 monomers bind to A $\beta$ 42 fibril surfaces, inhibiting secondary nucleation

In SI Sec. S5 we nondimensionalize Eqs. (8)-(10) and demonstrate that they satisfy the conditions for applicability of the general solution Eq. (7). In SI Secs. S6 A and S7 this is then used to calculate the explicit solution Eq. (S86). In the absence of seed, this simplifies to:

$$\frac{M_a(t)}{m_a(0)} = 1 - \left[ 1 + \frac{\varepsilon_a}{c_a} (e^{\kappa_a t} + e^{-\kappa_a t} - 2) \right]^{-c_a}, \quad (13a)$$

$$c_a = \frac{3}{2n'_2(a) + 1}, \quad \varepsilon_a = \frac{\alpha_{1,a}(m_{\text{tot},a})}{2m_{\text{tot},a}\alpha_{2,a}(m_{\text{tot},a})} \quad (13b)$$

$$\kappa_a = \sqrt{\alpha_{e,a}(m_{\text{tot},a})\alpha_{2,a}(m_{\text{tot},a})}, \quad (13c)$$

where  $n'_2(a)$  interpolates between  $n_2(a)$  and 0 depending on the degrees of saturation and inhibition, and is given by Eq. (S85). This solution is highly accurate; see Fig. S3a. As  $K_S(a)/m_{\text{tot},a}$  and  $K_S(ba)/m_{\text{tot},b} \rightarrow \infty$  (i.e. when initial monomer concentration is far below the saturation concentration), single-step kinetics are recovered as required.

It is known that, under the reaction conditions employed in the studies whose A $\beta$  alloform co-aggregation data we will revisit ([30, 34]), secondary nucleation of A $\beta$ 42 is saturated at all but the lowest monomer concentrations, with a dissociation constant of 1.1  $\mu\text{M}$  [46], and  $n_c = n_2 = 2$ . We confirmed these parameter values by fitting in SI Sec. S8 a standard saturating secondary nucleation model [6] to homogeneous A $\beta$ 42 aggregation experiments conducted in the same studies. Using these values, we then tested Eq. (13) against data for A $\beta$ 42-A $\beta$ 40 coaggregation and that for A $\beta$ 42-A $\beta$ 38 coaggregation, both truncated after the first sigmoid. Allowing inhibition only of primary nucleation by setting  $K_E(ba)^{-1} = K_S(ba)^{-1} = 0$  and fitting  $K_P(ba)$  (Fig. 3a), or only of elongation by setting  $K_P(ba)^{-1} = K_S(ba)^{-1} = 0$  and fitting  $K_E(ba)$  (Fig. 3b), yielded misfits. However, allowing inhibition only of secondary nucleation by setting  $K_P(ba)^{-1} = K_E(ba)^{-1} = 0$  and fitting  $K_S(ba)$  yielded good fits in both systems (Fig. 3c-d), providing strong evidence that at the concentrations investigated

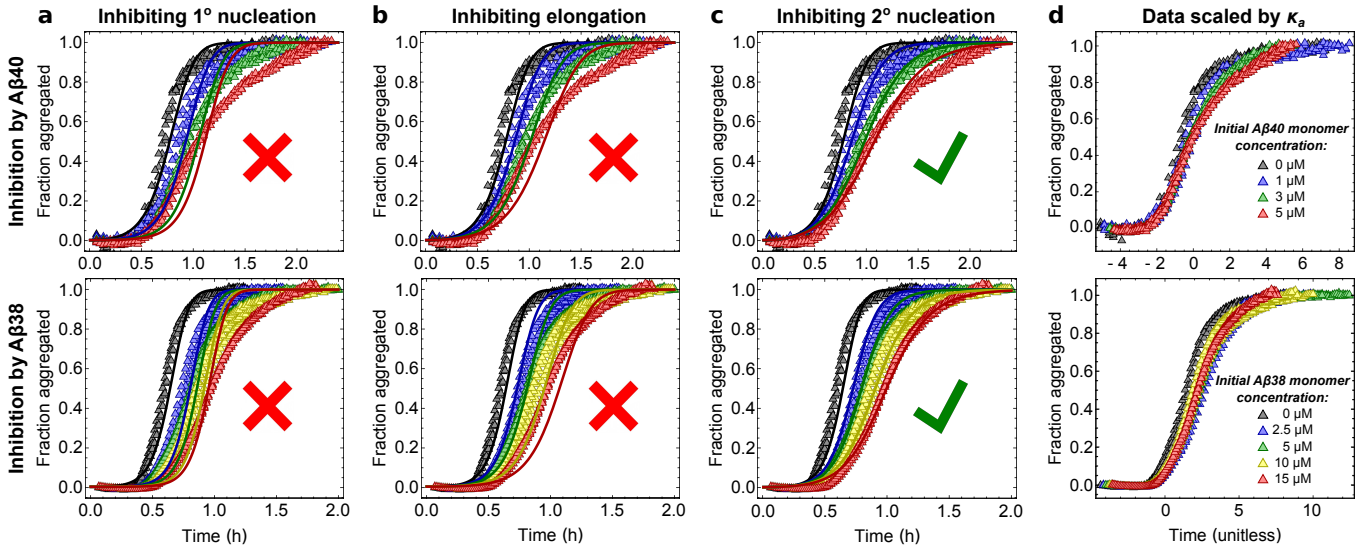


FIG. 3. Determining how A $\beta$ 42 fibril formation is inhibited by A $\beta$ 40 monomers (top) and A $\beta$ 38 monomers (bottom), by global fitting of kinetic models to first sigmoid of coaggregation data for 3  $\mu$ M A $\beta$ 42 monomer with various initial A $\beta$ xx monomer concentrations. **a**: Global misfit of model in which A $\beta$ xx inhibits primary nucleation (Eqs. (13) with  $K_E(ba)^{-1} = K_S(ba)^{-1} = 0$ ). **b**: Global misfit to models in which A $\beta$ xx inhibits elongation (Eqs. (13) with  $K_P(ba)^{-1} = K_S(ba)^{-1} = 0$ ). **c**: Global fit of model in which A $\beta$ xx inhibits secondary nucleation (Eqs. (13) with  $K_E(ba)^{-1} = K_P(ba)^{-1} = 0$ ). Fitted parameter values are summarized in Tables S2-S6. Identical patterns of fits and misfits are obtained when fitting these models to A $\beta$ 42-A $\beta$ 37 coaggregation data (Fig. S5). **d**: Scaling time by the inhibited secondary nucleation rates collapses the data onto a single curve, as expected if secondary nucleation is indeed the process inhibited.

here A $\beta$ xx monomers inhibit predominantly A $\beta$ 42 secondary nucleation. The apparent specificity of the inhibitory effect of A $\beta$ xx monomers to this step alone implies they achieve this effect by binding to the surface of A $\beta$ 42 fibrils. This follows since the other possible binding targets participating in secondary nucleation, oligomers and monomers, also participate in other reaction steps.

The dissociation constant  $K_S(ba)$  was found to be 0.39  $\mu$ M for A $\beta$ 40 monomer on A $\beta$ 42 fibrils, and 0.86  $\mu$ M for A $\beta$ 38 monomer on A $\beta$ 42 fibrils (compared to  $K_S = 1.1$   $\mu$ M for A $\beta$ 42 monomers). However, these values sit at or below the lowest initial monomer concentrations used; consequently, they are not well constrained and we can only conclude that they are sub- $\mu$ M [47]. There is therefore no evidence of differences in the affinities of these monomers towards A $\beta$ 42 fibrils.

### C. A $\beta$ 42 accelerates A $\beta$ 40 aggregation predominantly by enabling secondary co-nucleation

When A $\beta$ 42 aggregation is complete before that of the other peptide, Eq. (13) may be substituted for  $m_a(t)$  and  $M_a(t)$  in the rate laws for A $\beta$ xx fibril formation, Eqs. (11) (or Eq. (S86) when A $\beta$ 42 fibril seeds are present). In SI Sec. S5 they are nondimensionalized using timescale  $\kappa_b t$ , where  $\kappa_b = \sqrt{\alpha_{e,b}(m_{\text{tot},b})\alpha_{2,b}(m_{\text{tot},b})}$ . In SI Sec. S5 C we verify the applicability of the general solution Eq. (7) to Eqs. (11). In SI Secs. S6 A and S7 this is then used to calculate the following highly accurate approximate

solution (validated in Fig. S3):

$$\frac{M_b(t)}{m_b(0)} = 1 - \left[ 1 + \frac{\varepsilon_b}{c_b} (e^{\kappa_b t} + e^{-\kappa_b t} - 2) \right]^{-c_b} \quad (14a)$$

$$c_b = \frac{3}{2n'_2(b) + 1}, \quad \varepsilon_b = \frac{\alpha_{1,bb}(m_{\text{tot},b}) + \tilde{\alpha}_{ba}}{2m_{\text{tot},b}\alpha_{2,b}(m_{\text{tot},b})}, \quad (14b)$$

$$\tilde{\alpha}_{ba} = f_1\alpha_{1,ba}(m_{\text{tot},a}, m_{\text{tot},b}) + f_2\alpha_{2,ba}(m_{\text{tot},a}, m_{\text{tot},b}), \quad (14c)$$

where  $n'_2(b)$  is given by Eq. (S89) and interpolates between  $n_2(b)$  and 0 depending on the extent of saturation of secondary nucleation, similarly to  $n'_2(a)$ .  $\tilde{\alpha}_{ba}$  is a constant that expresses the contributions from primary and secondary co-nucleation to the effective total rate of primary nucleation of A $\beta$ xx fibrils. Co-nucleation enters nowhere else in the equation. Therefore, the only effect of co-nucleation is to translate second sigmoid in the kinetic curves corresponding to A $\beta$ xx fibrils to the left, as observed experimentally in refs. [30, 34]. The constants  $f_1$  and  $f_2$  are positive but  $< 1$  (see below, and SI Sec. S7), accounting for the faster reduction in co-nucleation rates than in A $\beta$ xx primary nucleation rates, caused by the faster depletion of A $\beta$ 42 monomer than of A $\beta$ xx monomer.

The dependence of the effective co-nucleation rate  $\tilde{\alpha}_{ba}$  on the A $\beta$ 42 seed concentrations  $M_a(0)$  and  $P_a(0)$  gives us a way to distinguish primary and secondary co-nucleation experimentally.  $f_1$  and  $f_2$  depend on seed con-

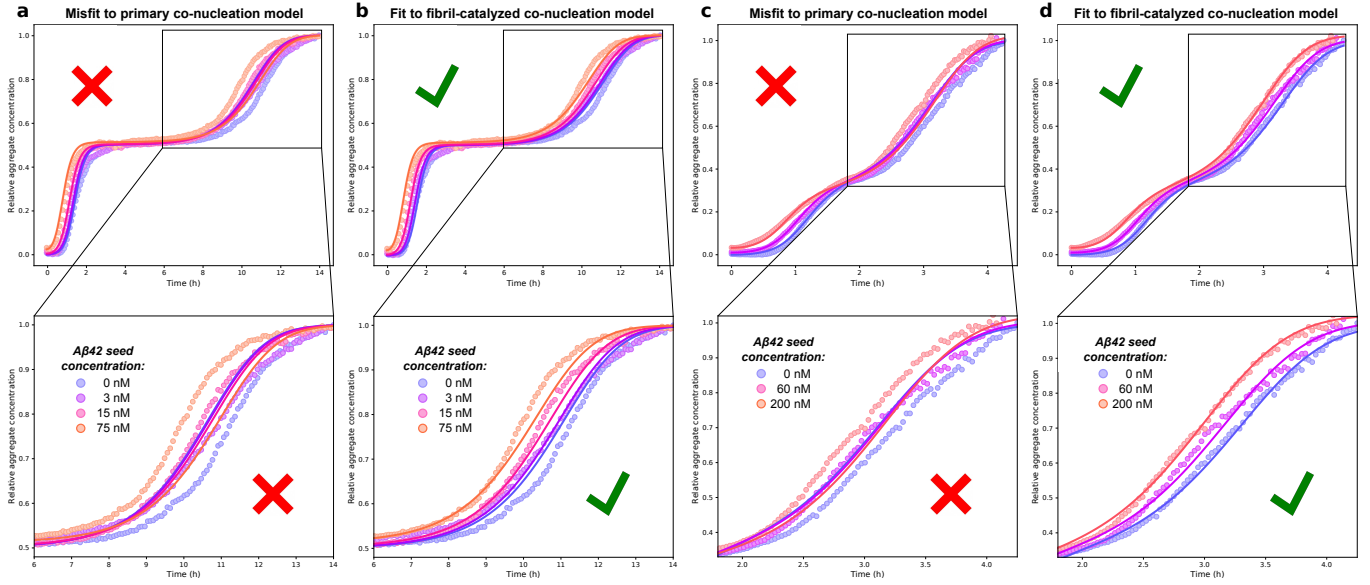


FIG. 4. Globally fitting the model (Eq. (16)) to kinetic data for co-aggregation of monomeric A $\beta$ 42 and A $\beta$ 40 with several concentrations of A $\beta$ 42 seeds identifies the mechanism of co-nucleation. **a-b**: Kinetic data from Fig. 7 of ref. [30], when processed to suppress noise, reveals a clear trend with increasing A $\beta$ 42 seed concentration (initial monomer concentrations both 1.5  $\mu$ M). **a**: Global misfit to full kinetic curves for A $\beta$ 42-A $\beta$ 40 coaggregation using model in which only primary co-nucleation occurs. **b**: Global fit to full dataset for A $\beta$ 42-A $\beta$ 40 coaggregation using model in which only secondary co-nucleation occurs (fitted parameter values are summarized in Table S3). A $\beta$ 42 fibril seed mass concentrations are 0 nM (blue), 3 nM (purple), 15 nM (pink), 75 nM (orange). **c-d**: To verify this result we repeated the experiment ourselves with different concentrations (2  $\mu$ M A $\beta$ 42 + 4  $\mu$ M A $\beta$ 40) and find the same trend. **c**: Model in which only primary co-nucleation occurs is again incapable of describing the data. **d**: Model in which only secondary co-nucleation occurs fits the data well globally (fitted parameter values are summarized in Table S4). A $\beta$ 42 fibril seed mass concentrations are 0 nM (blue), 60 nM (purple), 200 nM (orange).

centrations as follows:

$$f_1 = 1 - \left( 2\varepsilon_a + \frac{M_a(0)}{m_{\text{tot},a}} + \frac{2k_+(a)}{\kappa_a} P_a(0) \right)^{\frac{\kappa_b}{\kappa_a}} \bar{f}_1, \quad (15a)$$

$$f_1 = \left( 2\varepsilon_a + \frac{M_a(0)}{m_{\text{tot},a}} + \frac{2k_+(a)}{\kappa_a} P_a(0) \right)^{\frac{\kappa_b}{\kappa_a}} \bar{f}_2. \quad (15b)$$

$\bar{f}_1, \bar{f}_2 > 0$  are constants depending on the parameters entering the A $\beta$ 42 aggregation rate equations, whose precise forms are given in Eqs. (S90). Crucially, as seed concentrations  $M_a(0)$  and  $P_a(0)$  are raised,  $f_2$  increases but  $f_1$  decreases. So if A $\beta$ 42 influences A $\beta$ xx kinetics via primary co-nucleation ( $\varepsilon_{2,ba} = 0$ ), increasing A $\beta$ 42 seed concentrations should decrease co-nucleation overall and delay the second sigmoid to later times. Conversely, if A $\beta$ 42 influences A $\beta$ xx kinetics via secondary co-nucleation ( $\varepsilon_{1,ba} \ll \varepsilon_{2,ba}$ ), increasing A $\beta$ 42 seed concentrations should accelerate A $\beta$ xx aggregation and shift the second sigmoid to earlier times.

An intuitive justification is as follows. The rate of secondary co-nucleation is proportional to A $\beta$ 42 fibril concentration so is promoted by A $\beta$ 42 seed addition, at least at low seed concentrations. However, the rate of primary co-nucleation is not directly dependent on A $\beta$ 42 fibril concentration. Instead, adding A $\beta$ 42 seed indirectly reduces the primary co-nucleation rate by accelerating A $\beta$ 42 aggregation, reducing the amount of time during

which both monomeric A $\beta$ 42 and A $\beta$ xx are simultaneously present.

While in previous work we correctly identified the formation of co-oligomers as the key step accelerating A $\beta$ xx aggregation [30], the proposal that this co-nucleation of A $\beta$ 42 and A $\beta$ xx is primary does not hold in our current, more complete analysis. The key observation that led to this proposal in [30] was an experiment monitoring the formation of A $\beta$ 40 fibrils during aggregation of a 1:1 mixture of A $\beta$ 42 and A $\beta$ 40 monomers with the addition of different concentrations of A $\beta$ 42 fibril seeds (Fig. 7A of ref. [30]). We concluded then that there was no dose-dependent effect on the rate of A $\beta$ 40 with varying A $\beta$ 42 seed. However, in light of the mechanistic conclusions obtained above by application of our new analytical solutions, we revisited these data. Applying more stringent data processing to remove noise (see Methods Sec. II E), a steady increase in the A $\beta$ 40 aggregation rate with A $\beta$ 42 seed concentration becomes apparent (Fig. 4a-b), as would be expected for secondary not primary co-nucleation.

To confirm that secondary co-nucleation dominates over primary co-nucleation, we first fitted Eq. (13) to the data truncated after the first sigmoid to determine A $\beta$ 42 aggregation rate constants for this particular experiment.

The overall kinetic curves are described by:

$$M(t) = \frac{M_a(t) + M_b(t)}{m_{\text{tot},a} + m_{\text{tot},b}}. \quad (16)$$

Using these parameters we could then test Eq. (16) with either primary or secondary co-nucleation rate constants set to zero against the full kinetic dataset, yielding fits or misfits respectively (Fig. 4a-b). To further confirm this finding we performed a new seeded coaggregation experiment using different monomer concentrations; again, fits and misfits revealed that only secondary co-nucleation is consistent with the data (Fig. 4c-d). Fitted parameters are given in Tables S3-S4.

The data for the highest seed concentration used in ref. [30] ( $M_a(0)/m_{\text{tot},a} = 0.25$ ) was excluded from our new analysis in Fig. 4a-b, because at this concentration the assumption of low seed concentration used to derive the analytical model is violated. The half-time of the second sigmoid of the kinetic curve in this excluded dataset is actually *increased* relative to the next-highest seed concentration; this is a key reason why no effect of A $\beta$ 42 seeds on coaggregation was recognized in previous analysis [30]. Qualitatively, however, this remains consistent with a secondary co-nucleation mechanism. It can be rationalized as being due to the rapid depletion of monomeric A $\beta$ 42 at such high seed concentrations outweighing the increased availability of A $\beta$ 42 fibril surface. It is also plausible that at such high A $\beta$ 42 fibril concentrations, a significant proportion of monomeric A $\beta$ 40 becomes bound to the A $\beta$ 42 fibril surfaces without nucleating [48], further slowing the kinetics of A $\beta$ 40 fibril formation.

#### D. Co-oligomer formation underpins both co-aggregation and cross-inhibition phenomena

Coaggregation of A $\beta$ 42 and A $\beta$ xx into mixed fibrils, rather than just mixed oligomers, has been convincingly ruled out under the physiologically relevant reaction conditions used in this study [30, 34]. Under these conditions it has also been convincingly ruled out that A $\beta$ 42 fibrils alone can catalyze the aggregation of A $\beta$ xx anywhere near as strongly as can monomeric A $\beta$ 42 under the physiologically relevant reaction conditions used in this study [30, 34]. In other words, the formation of pure A $\beta$ xx nuclei or oligomers is not strongly catalysed by A $\beta$ 42 fibril surfaces.

Instead, the formation of co-oligomers of A $\beta$ 42 and A $\beta$ xx has been both predicted theoretically [30, 34] as intermediates of new A $\beta$ xx fibril nucleation and observed experimentally [49, 50]. Our findings in this study that A $\beta$ 42 secondary nucleation is inhibited by A $\beta$ xx monomers and that A $\beta$ 42-A $\beta$ xx co-nucleation is promoted by A $\beta$ 42 fibrils can then be understood as both originating from the same phenomenon: the binding of A $\beta$ xx to catalytic sites for A $\beta$ 42 secondary nucleation on A $\beta$ 42 fibril surfaces. Given the sequence specificity of

secondary nucleation [51], and the fact that pure A $\beta$ xx monomer cannot easily nucleate from these sites, it seems likely that for A $\beta$ xx binding in the correct conformation for nucleation to occur to be possible, these sites must already be partially occupied by monomeric A $\beta$ 42. Upon A $\beta$ xx binding, pure A $\beta$ 42 oligomers can no longer be nucleated at these catalytic sites. However, subsequently mixed A $\beta$ 42-A $\beta$ xx oligomers (or other fibril nucleation intermediates) can be formed. The inhibitory effect on A $\beta$ 42 secondary nucleation comes from the rate of formation of these intermediates and / or their propensity to convert into fibrils of A $\beta$ 42 morphology being much slower than for pure A $\beta$ 42 oligomers. The promotion of heterogeneous nucleation of A $\beta$ xx fibrils comes from these small heteromolecular intermediates having either a greater formation rate or a greater propensity to convert to fibrils of A $\beta$ xx morphology than do pure A $\beta$ xx nucleation intermediates via primary nucleation.

An alternative although closely related unified explanation for the observed coaggregation phenomena is that A $\beta$ xx monomer binds instead to A $\beta$ 42 oligomers after they have already detached from fibrils, not while they are still assembling on fibrils, and then only affects the conversion step in the manner discussed above. It is also plausible that A $\beta$ xx monomer binds to A $\beta$ 42 oligomers both before and after their detachment. In either case, this model would be equally consistent with the available kinetic data presented here and in earlier studies.

However, the first model is arguably more consistent with published experimental results showing A $\beta$ 42 fibrils being coated with A $\beta$ 40 monomers. For example, A $\beta$ 42 fibrils with added A $\beta$ 40 monomer are better dispersed and provide better contrast in cryo-TEM compared to pure A $\beta$ 42 fibrils [52]. Moreover, the results of SPR experiments show that A $\beta$ 40 monomers fail to elongate immobilized A $\beta$ 42 fibrils, yet a saturable binding curve is observed suggesting the binding of A $\beta$ 40 monomers to the sides of A $\beta$ 42 fibrils [48]. Nonetheless, this is not conclusive proof of the first model. Only the binding to the relatively rare catalytic sites for nucleation [53] is directly relevant, which cannot be distinguished by such experiments from binding to non-catalytic regions of the fibril surface. Although beyond the scope of the present paper, establishing a feasible experimental approach to distinguish these closely related mechanisms could be a productive research direction for future studies.

To validate our mechanistic model as conclusively as possible, we finally fitted Eq. (16) to unseeded full-timecourse kinetic data featuring multiple different monomeric protein concentrations for both A $\beta$ 42+A $\beta$ 40 co-aggregation (data from ref. [30]) and A $\beta$ 42+A $\beta$ 38 co-aggregation (data from ref. [34]). (Beforehand, we fitted Eq. (13) to the data truncated after the first sigmoid to obtain the inhibited A $\beta$ 42 aggregation rate constants independently.) Not allowing for any co-nucleation by imposing  $k_n(ab) = k_2(ab) = 0$  yielded a clear misfit to the A $\beta$ 42+A $\beta$ 40 co-aggregation data (Fig. 5a), verifying the importance of co-nucleation. Allowing  $k_2(ab) \neq 0$

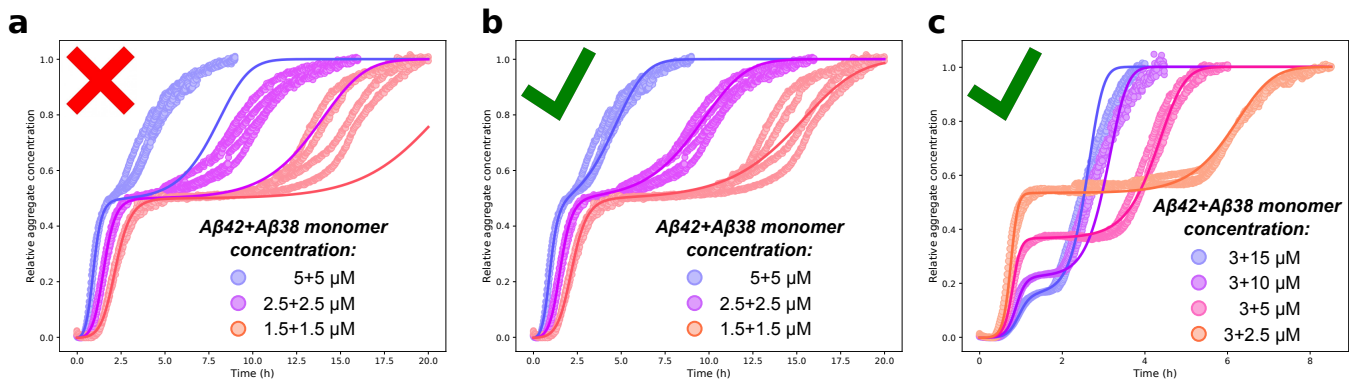


FIG. 5. Globally fitting the model (Eq. (16)) to full kinetic curves for multiple initial concentrations of monomeric  $A\beta_{xx}$  confirms the importance of co-nucleation. **a**: Global misfit to full dataset for  $A\beta_{42}$ - $A\beta_{40}$  coaggregation using model in which no co-nucleation occurs. **b**: Global fit to full dataset for  $A\beta_{42}$ - $A\beta_{40}$  coaggregation using model in which secondary co-nucleation occurs; fitted parameter values are summarized in Table S5. **c**: Global fit to full dataset for  $A\beta_{42}$ - $A\beta_{38}$  coaggregation using model in which co-nucleation occurs; fitted parameter values are summarized in Table S6.

then yielded good fits to both the full  $A\beta_{42}$ - $A\beta_{40}$  dataset (Fig. 5b) and the full  $A\beta_{42}$ - $A\beta_{38}$  dataset (Fig. 5c), and the fitted rates of co-nucleation confirmed the predictions of refs. [30, 34] that co-nucleation produces new  $A\beta_{xx}$  fibrils much faster than self-nucleation of  $A\beta_{xx}$ . (Reproducibility of the second sigmoid of  $A\beta_{42}$ - $A\beta_{37}$  co-aggregation data was too low to permit global fitting [34].)

#### IV. DISCUSSION

An implication of our finding that  $A\beta_{42}$  fibrils promote  $A\beta_{40}$  aggregation is that  $A\beta_{42}$  fibril formation may be upstream in the *in vivo* formation of fibrils consisting of the much more common  $A\beta_{40}$ . Should this apply to the interaction of  $A\beta_{42}$  with other peptides, then the relatively rapid  $A\beta_{42}$  fibril formation may be upstream in the formation of a number of other kinds of fibrils. As well as providing a possible mechanistic link between different amyloid diseases, it raises interesting questions as whether the morphology of the fibrils of other peptides could under certain circumstances be influenced by the morphology of  $A\beta_{42}$  fibrils. Given the lack of change in elongation and secondary nucleation rate constants for  $A\beta_{xx}$  fibrils formed in the presence of  $A\beta_{42}$ , a changed morphology for  $A\beta_{xx}$  fibrils seems unlikely under the conditions studied here. However, if the formation of fibrils of other kinds of peptides can be promoted by  $A\beta_{42}$  fibrils in the same way, then this possibility should be considered.

Our discovery that co-nucleation of new  $A\beta_{xx}$  fibrils via heteromolecular  $A\beta_{42}$ - $A\beta_{xx}$  intermediates occurs predominantly on  $A\beta_{42}$  fibril surfaces rather than in solution should perhaps not be surprising in hindsight, given that pure  $A\beta_{42}$  or  $A\beta_{40}$  nucleation also occurs predominantly on fibril surfaces. That such intermediates are formed predominantly by secondary nucleation

rather than primary nucleation, in competition with pure  $A\beta_{42}$  intermediates simultaneously explains both the acceleration of  $A\beta_{xx}$  nucleation by  $A\beta_{42}$  and the inhibition of  $A\beta_{42}$  secondary nucleation by  $A\beta_{xx}$ . Occam's razor therefore lends further support to our mechanistic interpretation of the co-aggregation and cross-inhibition effects over other potential mechanisms (such as primary co-nucleation with inhibition of elongation) that would generally rely on two distinct microscopic phenomena.

Our findings also provide a possible route to reconcile seemingly conflicting results in the literature regarding cross-seeding. In ref. [30] it was shown that  $A\beta_{42}$  fibrils alone cannot seed aggregation of  $A\beta_{40}$  monomer. Yet, numerous other studies have found at least a weak cross-seeding effect between these peptides [31]. Our results imply that even a small amount of monomeric  $A\beta_{42}$  monomer (or potentially some other  $A\beta$  variant) present as an impurity in such reactions could trigger cross-seeding. There are multiple ways such impurities could appear, including e.g., disaggregation of a fraction of the  $A\beta_{42}$  seed fibrils due to storage at low temperature where their solubility is higher, or length and sequence variants inevitably present in synthetic  $A\beta_{42}$  batches. Although other explanations for cross-seeding differences exist, such as differences in reaction conditions, the unintended presence of monomeric peptide impurities should be considered as a possible candidate.

Beyond  $A\beta_{42}$ - $A\beta_{xx}$  coaggregation, our mathematical method can solve the majority of plausible rate equations for protein aggregation, provided that the kinetics for the system of interest are sigmoidal in character. Additionally, the general solution we have derived is valid for a large proportion of these rate equations. Although the mathematical justification of the technique is challenging, being rooted in a little-known sub-field of the specialized field of Lie symmetry analysis of differential equations, its practical formulation is straightforward. The remarkably simple form of the solutions it produces per-

mits easy analysis of the kinetics. Alongside the lack of alternatives for solving more complicated protein aggregation rate equations, we expect these factors will result in widespread adoption of this new method. It should find immediate application in the analysis of kinetic experiments in other more complex biochemical systems involving protein aggregation in model mixtures, in vivo or in body fluids, and in the search for drugs that can inhibit critical reaction steps in this process. In fact, it has already been unwittingly employed on at least two occasions in the literature. Both the solution presented in ref. [8] for unsaturated single-peptide aggregation kinetics, and the universal solutions presented in ref. [9] for the kinetics of protein aggregation in which any participating reaction step can undergo enzyme-like saturation, were derived by matching perturbation series, in accordance with the method presented here. These derivations were justified at the time by making an analogy to renormalization group. However, our findings above demonstrate that they actually relied implicitly on the systems' asymptotic symmetry properties, not on renormalization group.

In summary, we have introduced a novel mathematical approach to solving nonlinear rate equations of a kind frequently encountered in self-assembly reactions. We have applied it to derive integrated rate laws for the co-aggregation of A $\beta$ 42 with other amyloidogenic peptides, which is a key event in Alzheimer's disease. By glob-

ally fitting these rate laws to experimental data, we have developed a detailed mechanistic understanding of these reactions under physiologically relevant conditions. We have revealed that A $\beta$ 42 fibril formation is inhibited by the binding of A $\beta$ 40 and A $\beta$ 38 to A $\beta$ 42 fibril surfaces, inhibiting secondary nucleation of new A $\beta$ 42 fibrils. We have also found that formation of co-oligomers of A $\beta$ 42 and A $\beta$ 40 is catalyzed by these same A $\beta$ 42 fibril surfaces, which ultimately stimulate the formation of fibrils consisting purely of these other peptides. Although no data are currently available to prove it, it seems likely both on physical chemistry grounds and by analogy with A $\beta$ 40 that the same holds for the formation of co-oligomers of A $\beta$ 42 and A $\beta$ 38.

## ACKNOWLEDGMENTS

We acknowledge support from the Lindemann Trust Fellowship, English-Speaking Union (AJD), the Swedish Research Council (SL), the MacArthur Foundation (LM), the Simons Foundation (LM) and the Henri Seydoux Fund (LM). The research leading to these results has received funding from the European Research Council under the European Union's Seventh Framework Programme (FP7/2007-2013) through the ERC grants PhysProt (agreement no. 337969), MAMBA (agreement no. 340890) and NovoNordiskFonden (SL).

- 
- [1] F. Chiti and C. M. Dobson, *Annu. Rev. Biochem.* **75**, 333 (2006).
- [2] F. Chiti and C. M. Dobson, *Annu. Rev. Biochem.* **86**, 27 (2017), pMID: 28498720, <https://doi.org/10.1146/annurev-biochem-061516-045115>.
- [3] T. P. J. Knowles, C. A. Waudby, G. L. Devlin, S. I. A. Cohen, A. Aguzzi, M. Vendruscolo, E. M. Terentjev, M. E. Welland, and C. M. Dobson, *Science* **326**, 1533 (2009).
- [4] S. I. A. Cohen, M. Vendruscolo, M. E. Welland, C. M. Dobson, E. M. Terentjev, and T. P. J. Knowles, *J. Chem. Phys.* **135**, 065105 (2011).
- [5] S. I. A. Cohen, M. Vendruscolo, C. M. Dobson, and T. P. J. Knowles, *J. Chem. Phys.* **135**, 065106 (2011).
- [6] G. Meisl, X. Yang, E. Hellstrand, B. Frohm, J. B. Kirkegaard, S. I. A. Cohen, C. M. Dobson, S. Linse, and T. P. J. Knowles, *Proc. Natl. Acad. Sci. U.S.A.* **111**, 9384 (2014), <http://www.pnas.org/content/early/2014/06/16/1401564111.full.pdf+html>.
- [7] T. C. T. Michaels, S. I. A. Cohen, M. Vendruscolo, C. M. Dobson, and T. P. J. Knowles, *Phys. Rev. Lett.* **116**, 038101 (2016).
- [8] T. C. T. Michaels, A. J. Dear, and T. P. J. Knowles, *Phys. Rev. E* **99**, 062415 (2019).
- [9] A. J. Dear, G. Meisl, T. C. T. Michaels, M. R. Zimmermann, S. Linse, and T. P. J. Knowles, *J. Chem. Phys.* **152**, 045101 (2020), <https://doi.org/10.1063/1.5133635>.
- [10] G. Meisl, J. B. Kirkegaard, P. Arosio, T. C. T. Michaels, M. Vendruscolo, C. M. Dobson, S. Linse, and T. P. J. Knowles, *Nat. Protoc.* **11**, 252 (2016).
- [11] G. Meisl, C. K. Xu, J. D. Taylor, T. C. T. Michaels, A. Levin, D. Otzen, D. Klenerman, S. Matthews, S. Linse, M. Andreasen, and T. P. J. Knowles, *Science Advances* **8**, eabn6831 (2022), <https://www.science.org/doi/pdf/10.1126/sciadv.abn6831>.
- [12] S. I. A. Cohen, S. Linse, L. M. Luheshi, E. Hellstrand, D. A. White, L. Rajah, D. E. Otzen, M. Vendruscolo, C. M. Dobson, and T. P. J. Knowles, *Proc. Natl. Acad. Sci. U.S.A.* **110**, 9758 (2013), <http://www.pnas.org/content/early/2013/05/22/1218402110.full.pdf>.
- [13] D. C. Rodriguez Camargo, E. Sileikis, S. Chia, E. Axell, K. Bernfur, R. L. Cataldi, S. I. A. Cohen, G. Meisl, J. Habchi, T. P. J. Knowles, M. Vendruscolo, and S. Linse, *ACS Chem. Neurosci.* **12**, 4406 (2021), pMID: 34783519, <https://doi.org/10.1021/acschemneuro.1c00454>.
- [14] J. Yang, A. J. Dear, T. C. T. Michaels, C. M. Dobson, and T. P. J. Knowles, S. Wu, and S. Perrett, *J. Am. Chem. Soc.* **140**, 2493 (2018), pMID: 29357227, <https://doi.org/10.1021/jacs.7b10439>.
- [15] M. Andreasen, G. Meisl, J. D. Taylor, T. C. T. Michaels, A. Levin, D. E. Otzen, M. R. Chapman, C. M. Dobson, S. J. Matthews, and T. P. J. Knowles, *mBio* **10**, 10.1128/mbio.02279 (2019), <https://journals.asm.org/doi/pdf/10.1128/mbio.02279-18>.
- [16] P. Arosio, M. Vendruscolo, C. M. Dobson, and T. P. J. Knowles, *Trends Pharmacol. Sci.* **35**, 127 (2014).

- [17] T. C. T. Michaels, A. Šarić, G. Meisl, G. T. Heller, S. Curk, P. Arosio, S. Linse, C. M. Dobson, M. Vendruscolo, and T. P. J. Knowles, *Proc. Natl. Acad. Sci. U.S.A.* **117**, 24251 (2020), <https://www.pnas.org/doi/pdf/10.1073/pnas.2006684117>.
- [18] T. C. Michaels, A. J. Dear, S. Cohen, M. Vendruscolo, and T. P. J. Knowles, *J. Chem. Phys.* **156**, 164904 (2022), [https://pubs.aip.org/aip/jcp/article-pdf/doi/10.1063/5.0077609/16542545/164904\\_1\\_online.pdf](https://pubs.aip.org/aip/jcp/article-pdf/doi/10.1063/5.0077609/16542545/164904_1_online.pdf).
- [19] G. Salvadó, K. Horie, N. R. Barthélemy, J. W. Vogel, A. Pichet Binette, C. D. Chen, A. J. Aschenbrenner, B. A. Gordon, T. L. S. Benzinger, D. M. Holtzman, J. C. Morris, S. Palmqvist, E. Stomrud, S. Janelidze, R. Ossenkoppele, S. E. Schindler, R. J. Bateman, and O. Hansson, *Nature Aging* **4**, 694 (2024).
- [20] A. J. Dear, D. Thacker, S. Wennmalm, L. Ortigosa-Pascual, E. A. Andrzejewska, G. Meisl, S. Linse, and T. P. J. Knowles, *ACS Chem. Neurosci.* **15**, 2296 (2024), pMID: 38785363, <https://doi.org/10.1021/acscchemneuro.4c00127>.
- [21] G. Brinkmalm, W. Hong, Z. Wang, W. Liu, T. T. O'Malley, X. Sun, M. P. Frosch, D. J. Selkoe, E. Portelius, H. Zetterberg, K. Blennow, and D. M. Walsh, *Brain* **142**, 1441 (2019), <https://academic.oup.com/brain/article-pdf/142/5/1441/28538153/awz066.pdf>.
- [22] M. P. Kummer and M. T. Heneka, *Alzheimer's Res. Ther.* **6**, 28 (2014).
- [23] S. Schilling, A. Pradhan, A. Heesch, A. Helbig, K. Blennow, C. Koch, L. Bertgen, E. H. Koo, G. Brinkmalm, H. Zetterberg, S. Kins, and S. Eggert, *Acta Neuropathol. Commun.* **11**, 87 (2023).
- [24] A. T. Welzel, J. E. Maggio, G. M. Shankar, D. E. Walker, B. L. Ostaszewski, S. Li, I. Klyubin, M. J. Rowan, P. Seubert, D. M. Walsh, and D. J. Selkoe, *Biochemistry* **53**, 3908 (2014).
- [25] O. Szczepankiewicz, B. Linse, G. Meisl, E. Thulin, B. Frohm, C. S. Frigerio, M. T. Colvin, A. C. Jacavone, R. G. Griffin, T. Knowles, D. M. Walsh, and S. Linse, *J. Am. Chem. Soc.* **137**, 14673 (2015).
- [26] J. T. Jarrett, E. P. Berger, and P. T. Lansbury, *Biochemistry (Mosc.)* **32**, 4693 (1993), pMID: 8490014, <https://doi.org/10.1021/bi00069a001>.
- [27] J. Wiltfang, H. Esselmann, P. Cupers, M. Neumann, H. Kretzschmar, M. Beyermann, D. Schleuder, H. Jahn, E. Rütther, J. Kornhuber, W. Annaert, B. De Strooper, and P. Saftig, *J. Biol. Chem.* **276**, 42645 (2001).
- [28] J. Näslund, A. Schierhorn, U. Hellman, L. Lanfelfelt, A. D. Roses, L. O. Tjernberg, J. Silbering, S. E. Gandy, B. Winblad, and P. Greengard, *Proc. Natl. Acad. Sci. U.S.A.* **91**, 8378 (1994), <https://www.pnas.org/doi/pdf/10.1073/pnas.91.18.8378>.
- [29] L. Gu and Z. Guo, *J. Neurochem.* **126**, 305 (2013), <https://onlinelibrary.wiley.com/doi/pdf/10.1111/jnc.12202>.
- [30] R. Cukalevski, X. Yang, G. Meisl, U. Weinger, K. Bernfur, B. Frohm, T. P. J. Knowles, and S. Linse, *Chem. Sci.* **6**, 4215 (2015).
- [31] J. Tran, D. Chang, F. Hsu, H. Wang, and Z. Guo, *FEBS Lett.* **591**, 177 (2017), <https://febs.onlinelibrary.wiley.com/doi/pdf/10.1002/1873-3468.12526>.
- [32] T. Weiffert, G. Meisl, P. Flagmeier, S. De, C. J. R. Dunning, B. Frohm, H. Zetterberg, K. Blennow, E. Portelius, D. Klenerman, C. M. Dobson, T. P. J. Knowles, and S. Linse, *ACS Chem. Neurosci.* **10**, 2374 (2019), pMID: 30793584, <https://doi.org/10.1021/acscchemneuro.8b00676>.
- [33] L. Cerofolini, E. Ravera, S. Bologna, T. Wiglenda, A. Böddrich, B. Purfürst, I. Benilova, M. Korsak, G. Gallo, D. Rizzo, L. Gonnelli, M. Fragai, B. De Strooper, E. E. Wanker, and C. Luchinat, *Chem. Commun.* **56**, 8830 (2020).
- [34] G. A. Braun, A. J. Dear, K. Sanagavarapu, H. Zetterberg, and S. Linse, *Chem. Sci.* **13**, 2423 (2022).
- [35] A. J. Dear, T. C. T. Michaels, and T. P. J. Knowles, *J. Chem. Phys.* **145**, 175101 (2016), <https://doi.org/10.1063/1.4966571>.
- [36] A. J. Dear and L. Mahadevan, arXiv (accepted for publication at *Proc. R. Soc. A*) **2309.05038** (2023), arXiv:2309.05038 [math-ph].
- [37] P. Olver, *Applications of Lie Groups to Differential Equations*, Graduate Texts in Mathematics (Springer New York, 2000).
- [38] Z. Toprakcioglu, A. Kamada, T. C. T. Michaels, M. Xie, J. Krausser, J. Wei, A. Saric, M. Vendruscolo, and T. P. J. Knowles, *Proc. Natl. Acad. Sci. U.S.A.* **119**, e2109718119 (2022), <https://www.pnas.org/doi/pdf/10.1073/pnas.2109718119>.
- [39] A. J. Dear, G. Meisl, C. G. Taylor, U. C. Palmiero, S. N. Stubbe, Q. Liu, P. Arosio, S. Linse, T. P. J. Knowles, and M. Andreasen, *Nanoscale*, (2024).
- [40] G. Barenblatt, *Similarity, Self-Similarity, and Intermediate Asymptotics* (Springer US, 2012).
- [41] C. M. Bender and S. A. Orszag, *Advanced Mathematical Methods for Scientists and Engineers* (Springer, New York, 1999).
- [42] N. Ibragimov and V. Kovalev, *Approximate and Renorm-group Symmetries*, Nonlinear Physical Science (Springer Berlin Heidelberg, 2009).
- [43] D. M. Walsh, E. Thulin, A. M. Minogue, N. Gustavsson, E. Pang, D. B. Teplow, and S. Linse, *FEBS J.* **276**, 1266 (2009).
- [44] B. Kragelund and K. Skriver, *Intrinsically Disordered Proteins* (Springer, 2020).
- [45] T. C. T. Michaels, C. A. Weber, and L. Mahadevan, *Proc. Natl. Acad. Sci. U.S.A.* **116**, 14593 (2019), <https://www.pnas.org/content/116/29/14593.full.pdf>.
- [46] G. Meisl, X. Yang, B. Frohm, T. P. J. Knowles, and S. Linse, *Sci. Rep.* **6**, 18728 (2016).
- [47] G. Meisl, L. Rajah, S. A. I. Cohen, M. Pfammatter, A. Šarić, E. Hellstrand, A. K. Buell, A. Aguzzi, S. Linse, M. Vendruscolo, C. M. Dobson, and T. P. J. Knowles, *Chem. Sci.* **8**, 7087 (2017).
- [48] K. Brännström, T. Islam, A. L. Gharibyan, I. Iakovleva, L. Nilsson, C. C. Lee, L. Sandblad, A. Pamrén, and A. Olofsson, *J. Mol. Biol.* **430**, 1940 (2018).
- [49] M. Iljina, G. A. Garcia, A. J. Dear, J. Flint, P. Narayan, T. C. T. Michaels, C. M. Dobson, D. Frenkel, T. P. J. Knowles, and D. Klenerman, *Sci. Rep.* **6**, 28658 (2016).
- [50] M. Baldassarre, C. M. Baronio, L. A. Morozova-Roche, and A. Barth, *Chem. Sci.* **8**, 8247 (2017).
- [51] D. Thacker, K. Sanagavarapu, B. Frohm, G. Meisl, T. P. J. Knowles, and S. Linse, *Proc. Natl. Acad. Sci. U.S.A.* **117**, 25272 (2020), <https://www.pnas.org/doi/pdf/10.1073/pnas.2002956117>.
- [52] M. Törnquist, R. Cukalevski, U. Weinger, G. Meisl, T. P. J. Knowles, T. Leiding, A. Malmendal, M. Akke, and S. Linse, *Proc.*

- Natl. Acad. Sci. U.S.A. **117**, 11265 (2020), <https://www.pnas.org/doi/pdf/10.1073/pnas.1918481117>.
- [53] S. Curk, J. Krausser, G. Meisl, D. Frenkel, S. Linse, T. C. T. Michaels, T. P. J. Knowles, and A. Šarić, Proc. Natl. Acad. Sci. U.S.A. **121**, e2220075121 (2024), <https://www.pnas.org/doi/pdf/10.1073/pnas.2220075121>.
- [54] H. Stephani, *Differential Equations: Their Solution Using Symmetries*, edited by M. MacCallum (Cambridge University Press, 1990).
- [55] V. A. Baikov, R. K. Gazizov, and N. H. Ibragimov, *Matematicheskii Sbornik* **178**, 435 (1988).
- [56] V. F. Kovalev, V. V. Pustovalov, and D. V. Shirkov, J. Math. Phys. **39**, 1170 (1998), <https://doi.org/10.1063/1.532374>.
- [57] G. Gaeta, Journal of Physics A: Mathematical and General **27**, 437 (1994).
- [58] D. Levi and M. A. Rodríguez, EPL **80**, 60005 (2007).
- [59] A. Šarić, T. C. T. Michaels, A. Zacccone, T. P. J. Knowles, and D. Frenkel, J. Chem. Phys. **145**, 211926 (2016), <http://aip.scitation.org/doi/pdf/10.1063/1.4965040>.
- [60] A. J. Dear, A. Šarić, T. C. T. Michaels, C. M. Dobson, and T. P. J. Knowles, J. Phys. Chem. B **122**, 11721 (2018), PMID: 30336667, <https://doi.org/10.1021/acs.jpcc.8b07805>.
-

# Supporting Information: Molecular mechanism of A $\beta$ alloform co-aggregation

## S1. INTRODUCTION TO LIE GROUP THEORY OF DIFFERENTIAL EQUATIONS

The theory of Lie groups finds diverse application across theoretical physics. It was originally developed by Sophus Lie as a systematic method for exactly solving nonlinear differential equations (DEs) by exploiting their symmetry properties; however, this application is largely unknown today. Consequently, it is widely believed that nonlinear DEs can be solved only by a combination of guesswork and ad-hoc methods of individually narrow applicability. In fact, most such methods may be derived from the Lie group theory of DEs, which provides a unified and general platform for solving DEs of any kind. Here we give a brief summary of those parts of Lie group theory of DEs that are utilized in the paper; for a more in-depth treatment, refs. [37, 54] can be consulted.

### A. Continuous transformations

A point transformation maps the independent and dependent variables  $x$  and  $y$  of the object being acted upon to  $\tilde{x}$  and  $\tilde{y}$ . Point transformations that are indexed by parameter  $s$  may be written  $\tilde{x} = \tilde{x}(x, y, s)$ ,  $\tilde{y} = \tilde{y}(x, y, s)$ . When these are also invertible, contain the identity at  $s = 0$ , and obey associativity via  $\tilde{x}(\tilde{x}(x, y, s), \tilde{y}(x, y, s), t) = \tilde{x}(x, y, s + t)$ , they form a one-parameter (or multi-parameter) group of point transformations. Because they are continuous, the infinitesimal transformation exists and can be accessed by expanding around  $s = 0$ :

$$\tilde{x}(x, y, s) = x + s \left. \frac{\partial \tilde{x}}{\partial s} \right|_{s=0} + \cdots = x + s \mathbf{X}x + O(s^2) \quad (\text{S1})$$

$$\tilde{y}(x, y, s) = y + s \left. \frac{\partial \tilde{y}}{\partial s} \right|_{s=0} + \cdots = y + s \mathbf{X}y + O(s^2), \quad (\text{S2})$$

where the operator  $\mathbf{X}$  is:

$$\mathbf{X} = \xi(x, y) \frac{\partial}{\partial x} + \eta(x, y) \frac{\partial}{\partial y}, \quad (\text{S3})$$

and the elements of the tangent vector  $(\xi(x, y), \eta(x, y))$  are:

$$\xi(x, y) = \left. \frac{\partial \tilde{x}}{\partial s} \right|_{s=0}, \quad \eta(x, y) = \left. \frac{\partial \tilde{y}}{\partial s} \right|_{s=0}. \quad (\text{S4})$$

The operator  $\mathbf{X}$  is the infinitesimal generator of the point transformation. Integrating the tangent vector over  $s$  will yield a finite transformation.

### B. What is a Lie symmetry?

A Lie symmetry of an object is a continuous transformation that leaves the object invariant. A rotational symmetry of a square is not a Lie symmetry, as it is discrete and can only be performed in multiples of  $\pi/2$  (Fig. S1a). However, a rotational symmetry of a circle can involve any angle, and is thus a Lie symmetry (Fig. S1b). A DE can be viewed as a geometrical object: a manifold consisting of the union of all possible solutions. Often such DEs possess Lie point symmetries: transformations of the dependent and independent variables that leave the overall manifold invariant. Applied to a particular solution (that spans a subspace of the DE manifold) a Lie symmetry of the DE transforms it into another solution (see Fig. S1c). By analogy, a rotational Lie symmetry maps a circle to itself but maps a point on the circle to another point.

The ability to express a Lie symmetry in infinitesimal form also makes it possible to calculate systematically the Lie point symmetries possessed by a given object. For DEs this procedure, although algorithmic, can be extremely long-winded because derivatives are not transformed in a straightforward way by Lie point symmetries. To avoid dozens or hundreds of pages of working, it is thus best implemented using computer algebra systems (CAS). On the other hand, for objects without derivatives the procedure is simple. For example, the circle in Fig. S1b may be expressed in polar coordinates as  $F = r - c = 0$ . In these co-ordinates the generator is  $\mathbf{X} = \xi_r \partial / \partial r + \xi_\theta \partial / \partial \theta$ . Trivially, solving  $\mathbf{X}F = 0$  yields  $\xi_r = 0$  and arbitrary  $\xi_\theta$ : a rotational symmetry. In cartesian co-ordinates  $F = x^2 + y^2 - c$ , and solving  $\mathbf{X}F = 0$  yields  $\eta$  in terms of  $\xi$ , giving the generator as follows:

$$0 = \mathbf{X}F = \left( \xi(x, y) \frac{\partial}{\partial x} + \eta(x, y) \frac{\partial}{\partial y} \right) (x^2 + y^2 - c) \quad (\text{S5})$$

$$\therefore \mathbf{X} = \xi(x, y) \left( y \frac{\partial}{\partial x} - x \frac{\partial}{\partial y} \right). \quad (\text{S6})$$

The arbitrary rotational transformation is recovered in cartesian coordinates as expected.

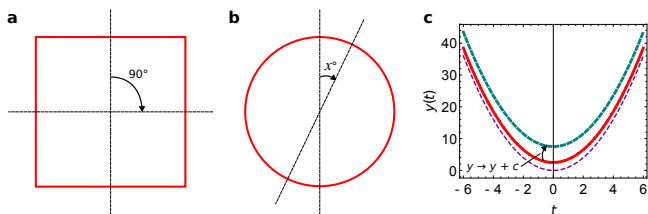


FIG. S1. An overview of Lie symmetries. **a**: Squares have discrete rotational symmetries. These cannot be reduced to infinitesimal form; therefore, they are not Lie symmetries. **b**: Circles can be rotated by any amount; rotation is thus a Lie symmetry of the circle. **c**: In general, symmetries of DEs map solutions to other solutions with different boundary conditions. An arbitrary translation on the  $y$  axis is a Lie symmetry of the DE  $\dot{y} = 2t$ , because this is solved by  $y = t^2 + c$ , and the translation just changes the value of  $c$ , giving the solution to the DE for new boundary conditions.

### C. Approximate symmetries

A more recent development in the field of Lie group analysis of DEs is the discovery that perturbed DEs can possess “approximate symmetries” [55]. These leave a perturbed DE invariant only to some finite order in the perturbation parameter  $\varepsilon$ . They can be identified by solving:

$$(\mathbf{X}^{(0)} + \varepsilon \mathbf{X}^{(1)} + \dots)(F_0 + \varepsilon F_1)|_{F_0 + \varepsilon F_1 = 0} = 0, \quad (\text{S7})$$

order-by-order [42]. They can often be used to find approximate solutions to perturbed DEs. However, approximate symmetries of DEs are more difficult to compute than exact symmetries, and there exist few if any CAS implementations of the procedure.

### D. Perturbation symmetries

Lie point symmetries of a DE are traditionally thought of as transformations acting on its dependent and independent variables. However, there is nothing to stop us pretending that the perturbation parameter  $\varepsilon$  in a perturbed DE is an independent variable, and searching for symmetries that act on  $\varepsilon$  as well [56]. Doing so can significantly extend the power of the Lie group approach. We have previously termed these “perturbation symmetries” (See ref. [36] for a detailed explanation of these symmetries and this choice of terminology).

Crucially, if a reference solution is known for the perturbation problem with  $\varepsilon = 0$ , this may be converted using a perturbation symmetry of the general solution into a solution valid for arbitrary  $\varepsilon$ . This is because such a symmetry leaves the space of solutions for all possible  $\varepsilon$  unchanged. Thus, acting on a solution for a specific  $\varepsilon$  maps it to another solution with a different  $\varepsilon$ .

Unfortunately, both exact and approximate perturbation symmetries are often extremely difficult or impossible to compute, due to the high dimensionality of the

manifold, which defeats most or all CAS implementations. However, we recently developed a method (explained in detail in [36]) that can compute approximate perturbation symmetries of the *solution* to a perturbed DE directly, with far greater ease than earlier methods.

## S2. METHOD OF ASYMPTOTIC LIE SYMMETRIES FOR SOLVING PROTEIN AGGREGATION KINETICS

### A. Exact, approximate and asymptotic Lie symmetries in protein aggregation

The simplest possible instance of protein aggregation kinetics described by equations of the form of Eqs (3) are exemplified by the kinetics of pure A $\beta$ 42 aggregation at pH 8.0, which obey:

$$\frac{d\Pi}{d\tau} = 2\varepsilon\mu(\tau)^{n_c} + \mu(\tau)^{n_2}(1 - \mu(\tau)) \quad (\text{S8a})$$

$$\frac{d\mu}{d\tau} = -\mu(\tau)\Pi(\tau). \quad (\text{S8b})$$

These (and many other instances of Eqs (3)) can be integrated once analytically, and subsequently reduced to quadrature [7]. However, the integration cannot be performed analytically. So, an exact analytic solution for  $\mu$  is not possible, and Eqs (S8) should not possess any non-trivial exact symmetries other than those that yield this quadrature. This can be verified explicitly by their computation using CAS. The objective of a Lie symmetry approach must therefore instead be to derive an approximate analytic solution. However, their explicit computation reveals that Eqs (S8) have no non-trivial approximate symmetries (Fig. S2a) either.

Yet, these equations have several approximate analytical solutions, implying they possess some other kind of approximate symmetry property even if they do not possess formal approximate symmetries. Given that these approximate solutions all become more accurate in the limit  $\mu \rightarrow 1$ , we consider the possibility of Lie symmetries that become exact only *asymptotically* in a given region of phase space (Fig. S2b). The concept of exact “asymptotic symmetries” of DEs, involving dependent and independent variables only, has been investigated in at least two prior mathematical papers [57, 58]. However, a systematic method for their computation was not established, and instead they were computed by guesswork from the DE and its exact symmetries. Hereafter we adopt the name “asymptotic” proposed in these papers for this class of symmetries.

Now, we propose asymptotic symmetries of *solutions* to DEs rather than of DEs themselves, and acting on all parameters in the problem, not just the dependent and independent variables. We also propose a systematic method for their computation. If a local approximation to the solution of a DE is available (such as a local perturbation series), then exact or approximate symmetries of

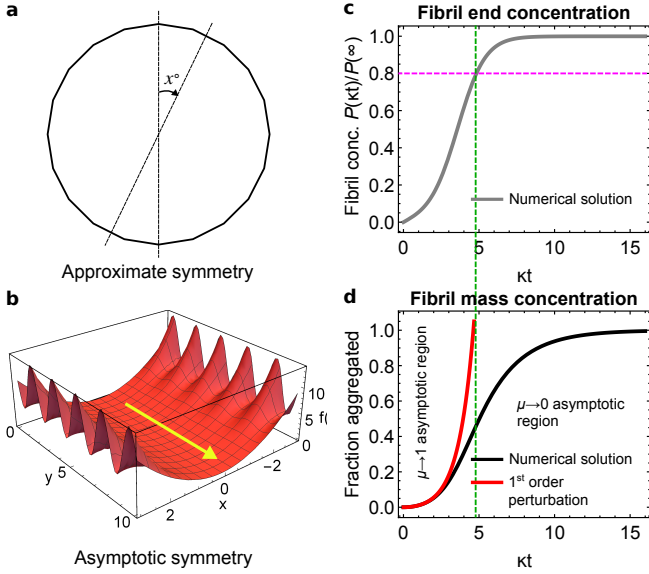


FIG. S2. Illustration of asymptotic symmetries, and asymptotic regions in the kinetics of linear protein self-assembly. **a**: Dodecagons are only approximately invariant under infinitesimal rotational transformations (to  $O(\varepsilon)$ , where  $\varepsilon \sim z \cos \theta$ , with  $\theta$  the external angle and  $z$  the side length), which are therefore an approximate Lie symmetry. **b**:  $f = x^2 + \varepsilon \sin(\pi y)x^5$  is asymptotically invariant to an arbitrary  $y$ -translation in the limit  $x \rightarrow 0$ ; such a translation is thus an asymptotic Lie symmetry. **c**: Numerical solution for normalized fibril end concentration  $\Pi$  (rate equation Eq. (S8a), gray); parameters are the same as in Fig. 1. **d**: Numerical solution for normalized fibril mass concentration  $1 - \mu$  (rate equation Eq. (S8b), black). The  $\mu \rightarrow 0$  asymptotic regime, dominated by simple exponential decay of  $\mu$ , is entered once the fibril number concentration begins to plateau. The local perturbation series (red, Eq. (6a)) is no longer valid in this regime.

this local approximation will be asymptotic symmetries of the solution to the DE. Since these approximations do not contain derivatives, computation of their Lie symmetries can easily be done by hand with no need for the usual computer algebra approaches.

Asymptotic symmetries computed from a local perturbation series are generally only valid near the initial or boundary conditions  $C_j(0)$ . They are clearly also only valid to the same order in the perturbation parameter as their parent series. (In principle, *exact* asymptotic solution symmetries can instead be calculated if local approximations are available that become exact approaching the phase point around which they were computed.) For example, solving Eqs (S8) perturbatively to first order with boundary conditions  $\{\mu(0) = 1 - \delta, \Pi(0) = \delta + O(\delta^2)\}$ , and using again indexing parameter  $s$ , yields the following local perturbation series for  $\mu$ :

$$\mu(\tau) = \mu^{(0)} + s\mu^{(1)} = 1 - s[\varepsilon(e^\tau + e^{-\tau} - 2) + \delta e^\tau]. \quad (\text{S9})$$

We can then seek from this a zeroth-order approximate

$\mu \rightarrow 1$  asymptotic perturbation symmetry for the exact solution to Eqs. (S8), acting solely on parameters  $\varepsilon$  and  $\delta$ :

$$\mathbf{X}_{\varepsilon, \delta}^{(0)} = \xi_\varepsilon^{(0)} \frac{\partial}{\partial \varepsilon} + \xi_\delta^{(0)} \frac{\partial}{\partial \delta} \quad (\text{S10})$$

Solving  $\mathbf{X}_{\varepsilon, \delta}^{(0)}(\mu^{(0)} + s\mu^{(1)}) = 0$  yields the zeroth-order symmetry:

$$\mathbf{X}_{\varepsilon, \delta}^{(0)} = \xi^{(0)} \left( e^\tau \frac{\partial}{\partial \varepsilon} - (e^\tau + e^{-\tau} - 2) \frac{\partial}{\partial \delta} \right), \quad (\text{S11})$$

where  $\xi^{(0)}$  is an arbitrary function of  $\varepsilon$  and  $\delta$ .

Finally, we propose that asymptotic perturbation symmetries may often remain approximately valid throughout the entire phase space of interest. If so, they may in principle be employed to find global approximate solutions. To evaluate whether a given such symmetry is indeed globally valid requires an examination of the bifurcations of the DEs. As discussed in the main text, for protein aggregation the phase space structure is simple, featuring only an attractive fixed point at  $\mu = 0$ . So, the global dynamics are partitioned into two asymptotic limits:  $\mu \rightarrow 1$  and  $\mu \rightarrow 0$  (Fig. S2c-d). The boundary between these regions of phase space is marked by the linearization of the kinetics.

$\mu \rightarrow 1$  asymptotic perturbation symmetries are then approximately valid globally under two circumstances. First, if the parameters transformed by the symmetry in response to an increase in the perturbation parameters drop out of the  $\mu \rightarrow 0$  kinetics at leading order. For example, Eqs. (S8) lose memory of the initial conditions  $\{\mu(0) = 1 - \delta, \Pi(0) = \delta + O(\delta^2)\}$  in the  $\mu \rightarrow 0$  asymptotic region, becoming independent of  $\delta$ . Thus, although the  $\mu \rightarrow 1$  asymptotic symmetry Eq. (S11) transforms  $\delta$  incorrectly here, it does not matter because the solution no longer depends on  $\delta$  in this limit, and so Eq. (S11) is actually universally valid to zeroth order in  $\varepsilon$ . The second circumstance is if the boundary between asymptotic regions is sufficiently close to  $\mu = 0$ , the second region may be neglected. We will see examples of this later.

## B. Special solution for $\varepsilon = d = 0$

When  $\alpha_1$ ,  $\alpha_2$  and  $\alpha_e$  are finite constants and  $\varepsilon = 0$ , Eqs. (3) reduce to:

$$\frac{d\Pi}{d\tau} = \mu(\tau)^{n_2}(1 - \mu(\tau)) \quad (\text{S12})$$

$$\frac{d\mu}{d\tau} = -\mu(\tau)\Pi(\tau). \quad (\text{S13})$$

Integrating once, with boundary conditions  $\mu(0) = 1 - \delta$ ,  $\Pi(0) = p$  yields for  $n_2 > 0$ :

$$\Pi(\tau) = \left( p^2 + 2 \frac{(1 - \delta)^{n_2} - \mu(\tau)^{n_2}}{n_2} - 2 \frac{(1 - \delta)^{n_2+1} - \mu(\tau)^{n_2+1}}{n_2 + 1} \right)^{1/2}. \quad (\text{S14})$$

$n_2 = 0$  is also possible and indicates fibril fragmentation rather than secondary nucleation. In this case, we instead obtain:

$$\Pi(\tau) = \left( p^2 - 2 \ln \frac{\mu}{1-\delta} - 2((1-\delta) - \mu(\tau)) \right)^{1/2}. \quad (\text{S15})$$

At this point, the problem is reduced to quadrature, with:

$$t = - \int_{1-\delta}^{\mu} \frac{d\mu}{\mu \Pi(\mu)}. \quad (\text{S16})$$

If we choose  $p = p_0(\delta) = \delta + O(\delta^2)$ , where:

$$p_0 = \sqrt{2 \frac{1 - (1-\delta)^{n_2}}{n_2} - 2 \frac{1 - (1-\delta)^{n_2+1}}{n_2+1}}, \quad (\text{S17})$$

then Eq. (S16) reduces to:

$$t = - \int_{1-\delta}^{\mu} \frac{d\mu}{\mu \left( 2 \frac{1-\mu^{n_2}}{n_2} - 2 \frac{1-\mu^{n_2+1}}{n_2+1} \right)^{1/2}}, \quad (\text{S18})$$

with the first term in the square root replaced by  $-2 \ln \mu$  if  $n_2 = 0$ . To evaluate this integral, it is necessary to find an accurate approximate expression  $g(\mu)$  for the denominator  $f(\mu)$ . We start by investigating  $f(\mu)$  in the interval  $[0, 1]$  containing all possible values of  $\mu$ . We find the following basic properties:

$$f(0) = f(1) = 0 \quad (\text{S19})$$

$$f(\mu) > 0, \quad 0 < \mu < 1 \quad (\text{S20})$$

$$f'(0) = c, \quad f'(1) = -1 \quad (\text{S21})$$

$$f''(\mu) \leq 0, \quad 0 \leq \mu \leq 1. \quad (\text{S22})$$

If we instead restrict our attention to the interval  $[0, 1-\delta]$ , with small positive  $\delta$ , we find furthermore that:

$$f(1-\delta) = \delta + O(\delta^2), \quad f'(1-\delta) = -1 + \frac{2n_2+4}{3}\delta + O(\delta^2). \quad (\text{S23})$$

Also, there is a single turning point (a maximum) in this interval. When  $n_2 = 1$  the maximum value is  $f_{\max} = 1/4$ , occurring at  $\mu_{\max} = 1/2$ . As  $n_2 \rightarrow \infty$ ,  $f_{\max} \rightarrow c$ , and occurs at  $\mu_{\max} \rightarrow 1$ . Taken together, these results indicate that  $f$  is a low hill, rising from 0 at either end of the interval  $[0, 1]$  to a value  $\leq 1/4$ . Thus neither  $f$  nor  $f'$  have poles.

Such simple behaviour should be adequately captured by the simple functional form:

$$g(\mu) = c_1 \mu^{p_1} + c_2 \mu^{p_2} + c_3, \quad p_2 > p_1 \geq 1. \quad (\text{S24})$$

This is fortunate, because more complicated polynomials in  $\mu$  are unlikely to lead to an integrable  $g^{-1}$ . Now we constrain the parameters in  $g$  by matching to the properties of  $f$ . First imposing  $g(0) = f(0) = 0$  requires  $c_3 = 0$ . Imposing  $g(1-\delta) = f(1-\delta) = \delta + O(\delta^2)$  then leads to  $c_2 = -c_1$  and  $p_2 - p_1 = 1/c_1 > 0$ , so  $g$  has the form:

$$g(\mu) = c_1 \mu^{p_1} \left( 1 - \mu^{1/c_1} \right). \quad (\text{S25})$$

To inherit the property that  $f'(0) > 0$  requires  $p_1 = 1$ . This is also fortunate, since otherwise  $g^{-1}$  would not be integrable. With this form of  $g$  we can already evaluate (and invert)  $t = \int_{1-\delta}^{\mu} g^{-1} d\mu$ , yielding:

$$\mu(\tau) = \frac{1}{(1 + e^t [(1-\delta)^{-1/c_1} - 1])^{c_1}}. \quad (\text{S26})$$

Our asymptotic symmetry transformation method requires that our special solution have the correct  $\mu \rightarrow 1$  asymptotic dynamics. Therefore, to choose  $c_1$ , we match  $g'(1-\delta) = f'(1-\delta)$  ( $g'(1)$  already equals  $f'(1) = -1$ ), yielding finally  $c_1 = 3/(2n_2 + 1)$ .

(If we had instead matched  $g'(0) = f'(0)$ , we would have obtained  $c_1 = \sqrt{2/(n_2(n_2+1))}$ . This would give a slightly more accurate solution for  $n_2 > 1$ , because for larger values of  $n_2$  secondary nucleation decreases significantly at a larger value of  $\mu$ , and the  $\mu \rightarrow 0$  region is more important to the overall dynamics. However, there is not a great difference between these choices for  $c_1$ , with the maximum difference of 6% attained as  $n_2 \rightarrow \infty$ .)

Since  $\delta \ll 1$ , Eq. (S26) reduces to:

$$\mu_0(\tau, c_1, \delta) = \frac{1}{(1 + \delta e^\tau / c_1)^{c_1}}, \quad (\text{S27a})$$

$$c_1 = \frac{3}{2n_2 + 1}. \quad (\text{S27b})$$

We will use this as the special solution throughout, taking advantage of its greater simplicity than the ‘‘exact’’ special solution.

### C. Regularizing local perturbation series using asymptotic symmetries

Globally valid perturbation symmetries can in principle be used to regularize a singular perturbation problem by transforming a known special solution, such as Eq. (S27), which is valid when  $\varepsilon = 0$ , for arbitrary  $\delta$ , and for  $p$  as a function of  $\delta$  satisfying  $p(\delta = 0) = 0$ . Since  $c_1$  does not enter into the  $\mu \rightarrow 1$  asymptotic dynamics Eq. (S9), a global solution to Eqs. (S8) for  $\delta = 0$  can be obtained simply by integrating the globally valid asymptotic perturbation symmetry Eq. (S11) from  $(0, \delta)$  to  $(\varepsilon, 0)$ :

$$\frac{d\varepsilon}{ds} = e^\tau, \quad \frac{d\delta}{ds} = -(e^\tau + e^{-\tau} - 2) \quad (\text{S28a})$$

$$\varepsilon = s e^\tau, \quad -\delta = -s(e^\tau + e^{-\tau} - 2) \quad (\text{S28b})$$

$$\therefore \delta \rightarrow \varepsilon(e^\tau + e^{-\tau} - 2)/e^\tau. \quad (\text{S28c})$$

Replacing  $\delta$  in Eq. (S27) accordingly yields:

$$\mu(\tau) = \frac{1}{\left( 1 + \frac{\varepsilon}{c_1} (e^\tau + e^{-\tau} - 2) \right)^{c_1}}, \quad (\text{S29})$$

with  $c_1$  defined as before.

The same special solution is often available for the more complicated Eqs. (3) with arbitrary initial conditions when  $\varepsilon = 0$  and  $p = p_0$  (with  $p_0$  a function of  $\delta$  given by Eq. (S17)). This requires that  $\alpha_1$ ,  $\alpha_2$  and  $\alpha_e$  depend on a parameter  $d$  in such a way that  $d = 0$  reduces them to finite constants. An asymptotic perturbation symmetry connecting  $(c_1, \delta)$  with  $(d, \varepsilon, p)$  may then be used to transform the special solution Eq. (S27) to a general solution to Eqs. (3).

Because this kind of symmetry does not transform the dependent and independent variables, a shortcut in this procedure may be taken: it is not necessary to explicitly compute the symmetry and its finite transformations. To see why, suppose such a symmetry connecting  $(c_1, \delta)$  with  $(d, \varepsilon)$  has been found. From these, finite transformations taking  $(\tilde{c}_1, \tilde{\delta}, 0, 0)$  to  $(c_1, \delta, d, \varepsilon)$  can be calculated. Whatever they may be, they can always be expressed in inverse form as  $\tilde{\delta} = g_\delta(\tau, c_1, \delta, d, \varepsilon)$ ,  $\tilde{c}_1 = g_{c_1}(\tau, c_1, \delta, d, \varepsilon)$  where a tilde over a parameter signifies it is at its pre-transformation value. Our global solution is then  $\mu_0(\tau, \tilde{c}_1, \tilde{\delta})$ . Now, since transforming one asymptotic expansion must yield another,  $g_\delta$  and  $g_{c_1}$  must satisfy:

$$\mu_{0,\text{asy}}(\tau, \tilde{c}_1, \tilde{\delta}) \equiv \mu_{\text{asy}}(\tau, c_1, \delta, d, \varepsilon), \quad (\text{S30})$$

where  $\mu_{0,\text{asy}}$  is the asymptotic expansion of the special solution  $\mu_0$  in this region of phase space, and  $\mu_{\text{asy}}(\tau, c_1, \delta, d, \varepsilon)$  is the asymptotic limit of the full dynamics in the same region (e.g. Eq. (6), or a higher-order series). So, the finite transformations can be identified by inspection of  $\mu_{\text{asy}}$ ; a globally valid solution is then obtained by substituting these transformations into Eq. (S27).

### S3. SOLUTION OF GENERAL PROTEIN AGGREGATION RATE EQUATIONS BY ASYMPTOTIC LIE SYMMETRY

#### A. Perturbative solution to second order

The general equations Eqs. (3) can be rewritten for simplicity as:

$$\frac{d\Pi}{d\tau} = 2s\varepsilon\tilde{\alpha}_1(t, \mu) + \tilde{\alpha}_2(\mu)(1 - \mu(\tau)) \quad (\text{S31a})$$

$$\frac{d\mu}{d\tau} = -\tilde{\alpha}_e(\mu)\Pi(\tau), \quad (\text{S31b})$$

$$\mu(0) = 1 - s\delta, \quad \Pi(0) = sp \quad (\text{S31c})$$

where  $\tilde{\alpha}_x(t, \mu) = \alpha_x(t, m_{\text{tot}}\mu)/\alpha_x(0, m_{\text{tot}})$ ,  $\varepsilon = \alpha_1(0, m_{\text{tot}})/(2m_{\text{tot}}\alpha_2(m_{\text{tot}}))$  and  $s$  is the perturbation bookkeeping parameter, the zeroth order perturbation solutions are, as outlined in the main text, given by:

$$\Pi^{(0)} = 0, \quad \mu^{(0)} = 1. \quad (\text{S32})$$

The first order perturbation equations are given by:

$$\frac{d\Pi^{(1)}}{d\tau} = 2\varepsilon\tilde{\alpha}_1(t, 1) - \mu^{(1)} \quad (\text{S33a})$$

$$\frac{d\mu^{(1)}}{d\tau} = -\Pi^{(1)}, \quad (\text{S33b})$$

$$\mu^{(1)}(0) = -\delta, \quad \Pi^{(1)}(0) = p. \quad (\text{S33c})$$

In the case of  $\alpha_1(t, m) \equiv \alpha_1(m)$ , they are solved by:

$$\Pi^{(0)} = 0, \quad \mu^{(0)} = 1 \quad (\text{S34a})$$

$$\Pi^{(1)} = \varepsilon(e^\tau - e^{-\tau}) + \frac{\delta}{2}(e^\tau - e^{-\tau}) + \frac{p}{2}(e^\tau + e^{-\tau}), \quad (\text{S34b})$$

$$\mu^{(1)} = -\varepsilon(e^\tau + e^{-\tau} - 2) - \frac{\delta}{2}(e^\tau + e^{-\tau}) - \frac{p}{2}(e^\tau - e^{-\tau}). \quad (\text{S34c})$$

For the remainder, of the section, however, we will not make this assumption. We instead consider the more general condition that the kinetics are secondary-dominated such that  $\alpha_1$  grows less rapidly with  $t$  than  $e^{\kappa t}$ . In this case, the particular integral of  $\mu^{(1)}$  will also grow less rapidly than  $e^\tau$ . We can then write the first order perturbation terms as:

$$\Pi^{(1)} = qe^\tau + \mathcal{R}, \quad \mu^{(1)} = -qe^\tau + \mathcal{R} \quad (\text{S35a})$$

$$q \equiv \mathcal{L}(\varepsilon, \delta, p), \quad (\text{S35b})$$

where  $\mathcal{R}$  consists of terms that diverge less rapidly with  $\tau$ , and  $\mathcal{L}$  denotes a linear function. (In the case that  $\alpha_1(t, m) \equiv \alpha_1(m)$ ,  $q = \varepsilon + \delta/2 + p/2$ .)

Now, consider the expansion in  $s$  of  $\tilde{\alpha}$ :

$$\tilde{\alpha} = 1 + s \left. \frac{d\tilde{\alpha}}{ds} \right|_{s=0} + O(s^2) = 1 + s \left. \frac{\partial \tilde{\alpha}}{\partial \mu} \frac{d\mu}{ds} \right|_{s=0} + O(s^2) \quad (\text{S36a})$$

$$= 1 + s\mu^{(1)} \left. \frac{\partial \tilde{\alpha}}{\partial \mu} \right|_{s=0} + O(s^2) \quad (\text{S36b})$$

$$= 1 + s\mu^{(1)}\tilde{\alpha}'(1) + O(s^2), \quad (\text{S36c})$$

where the prime indicates differentiation with respect to  $\mu$ . The second order perturbation equation is then:

$$\frac{d\Pi^{(2)}}{d\tau} = 2\varepsilon\mu^{(1)}\tilde{\alpha}'_1(1) - \mu^{(1)2}\tilde{\alpha}'_2(1) - \mu^{(2)} \quad (\text{S37a})$$

$$\frac{d\mu^{(2)}}{d\tau} = -\mu^{(1)}\tilde{\alpha}'_e(1)\Pi^{(1)} - \Pi^{(2)}, \quad (\text{S37b})$$

$$\mu^{(2)}(0) = \Pi^{(2)}(0) = 0. \quad (\text{S37c})$$

These can be combined into:

$$\frac{d^2\mu^{(2)}}{d\tau^2} - \mu^{(2)} = -\tilde{\alpha}'_e(1) \frac{d}{d\tau} \left( \mu^{(1)}\Pi^{(1)} \right) - 2\varepsilon\tilde{\alpha}'_1(1)\mu^{(1)} + \tilde{\alpha}'_2(1)\mu^{(1)2}. \quad (\text{S38})$$

The complementary function of  $\mu^{(2)}$  will be  $O(e^\tau)$ , as with  $\mu^{(1)}$ .

We seek the most-divergent terms of the second-order perturbation solution. These will be the  $O(e^{2\tau})$  components of the particular integral. These can be computed without the need for retaining the less-divergent parts of the inhomogeneous terms of Eq. (S38). With this simplification Eq. (S38) becomes:

$$\frac{d^2\mu^{(2)}}{d\tau^2} - \mu^{(2)} = 2q^2\tilde{\alpha}'_e(1)e^{2\tau} + q^2\tilde{\alpha}'_2(1)e^{2\tau}. \quad (\text{S39})$$

Its solution can therefore be written as:

$$\mu^{(2)} = \frac{q^2}{3}e^{2\tau}(\tilde{\alpha}'_2(1) + 2\tilde{\alpha}'_e(1)) + \mathcal{R}. \quad (\text{S40})$$

### B. Asymptotic symmetry transformation

To second order in  $s$ , the expansion of the special solution Eq. (S27) from the main text (where bookkeeping parameter  $s$  has again been introduced to pre-multiply  $\delta$ ) is:

$$\tilde{\mu}_2 = 1 - s\tilde{\delta}e^\tau + s^2\frac{\tilde{c}_1 + 1}{2\tilde{c}_1}\tilde{\delta}^2e^{2\tau} + O(\delta^3), \quad (\text{S41})$$

where we have already made the substitutions  $\delta \rightarrow \tilde{\delta}$  and  $c_1 \rightarrow \tilde{c}_1$ . Matching the first order perturbation solution requires the finite transformation<sup>2</sup>:

$$\tilde{\delta}e^\tau = -\mu^{(1)}(\tau) + O(s). \quad (\text{S42})$$

The expansion of the special solution is then:

$$\tilde{\mu}_2 = 1 - s\mu^{(1)} + s^2\frac{\tilde{c}_1 + 1}{2\tilde{c}_1}\mu^{(1)2} + O(s^3). \quad (\text{S43})$$

We can only in general match to second order the most-divergent terms in  $\tau$  (proportional to  $e^{2\tau}$ ), if we desire a simple, time-independent  $c_1$ . (There is no great purpose in seeking a time-dependent  $c_1$  since the  $\mu \rightarrow 1$  kinetics are already captured exactly by the first-order matching, and the asymptotic symmetry loses validity as  $t \rightarrow \infty$ .) The matching then requires:

$$\frac{\tilde{c}_1 + 1}{2\tilde{c}_1} = \frac{1}{3}(\tilde{\alpha}'_2(1) + 2\tilde{\alpha}'_e(1)) \quad (\text{S44a})$$

$$\frac{1}{\tilde{c}_1} = \frac{2}{3}(\tilde{\alpha}'_2(1) + 2\tilde{\alpha}'_e(1)) - 1 \quad (\text{S44b})$$

$$\Rightarrow \tilde{c}_1 = \frac{3}{2(\tilde{\alpha}'_2(1) + 2\tilde{\alpha}'_e(1)) - 3}. \quad (\text{S44c})$$

<sup>2</sup> We may in fact choose any transformation  $\tilde{\delta}$  whose first-order expansion satisfies this relation. This flexibility can be leveraged to satisfy the initial conditions exactly rather than to  $O(s^2)$  when seed is present, although we need not pursue this here where the seed concentration is very low.

To remove some superfluous terminology:

$$\tilde{\alpha}'_i(1) = \frac{d}{d\mu} \frac{\alpha_i(m)}{\alpha_i(m_{\text{tot}})} \Big|_{m=m_{\text{tot}}} \quad (\text{S45a})$$

$$= m_{\text{tot}} \frac{d}{dm} \frac{\alpha_i(m)}{\alpha_i(m_{\text{tot}})} \Big|_{m=m_{\text{tot}}} \quad (\text{S45b})$$

$$= m \frac{d}{dm} \ln \alpha_i(m) \Big|_{m=m_{\text{tot}}} \quad (\text{S45c})$$

$$= \frac{d \ln \alpha_i(m)}{d \ln m} \Big|_{m=m_{\text{tot}}} \quad (\text{S45d})$$

The general solution is then given by using the substitutions Eq. (S42) and Eq. (S44) on the special solution Eq. (S27). Setting  $s = 1$ , this gives:

$$\mu = \left(1 - \frac{\mu^{(1)}(\tau)}{c_1}\right)^{-c_1} \quad (\text{S46a})$$

$$c_1 = \left(\frac{2}{3} \frac{d \ln [\alpha_2(m)\alpha_e(m)^2]}{d \ln m} \Big|_{m=m_{\text{tot}}} - 1\right)^{-1}. \quad (\text{S46b})$$

### S4. KINETIC MODEL FOR AMYLOID FIBRIL FORMATION WITH SATURATING AND INHIBITED SECONDARY NUCLEATION

If type- $b$  monomers can compete with type- $a$  monomers for binding to secondary nucleation sites on type- $a$  fibrils, the total mass concentration of  $A\beta_{42}$  fibrils is:

$$M_a = M_a^f + M_a^a + M_a^b, \quad (\text{S47})$$

where  $M_a^f$  is the free (unbound) fibril mass concentration, and  $M_a^a$  and  $M_a^b$  are the mass concentrations of type- $a$  fibrils bound by types  $a$  and  $b$  monomers, respectively. If, as was done here, the simplifying assumption is made that pre-equilibrium is achieved between bound and unbound states, then we may write:

$$\frac{m_a^{n_2(a)} M_a^f}{M_a^a} = K_S(a)^{n_2(a)}, \quad \frac{m_b^{n_2(ba)} M_a^f}{M_a^b} = K_S(ba)^{n_2(ba)}, \quad (\text{S48})$$

where  $K_S(a)^{n_2(a)}$  and  $K_S(ba)^{n_2(ba)}$  are the equilibrium constants for the unbinding of types  $a$  and  $b$  monomers respectively from type- $a$  fibrils. Combining these equations allows us to express the total type- $a$  fibril mass concentration as:

$$M_a = M_a^f \left(1 + m_a^{n_2(a)}/K_S(a)^{n_2(a)} + (m_b/K_S(ba))^{n_2(ba)}\right). \quad (\text{S49})$$

Considering that the rate of generation of new type- $a$  fibrils by secondary nucleation is:

$$r_S = 2k_c M_a^a, \quad (\text{S50})$$

where  $k_c$  is some conversion rate constant, this ultimately yields:

$$r_S = \frac{2k_2(a)m_a(t)^{n_2(a)}M_a(t)}{1 + (m_a(t)/K_S(a))^{n_2(a)} + (m_b(0)/K_S(ba))^{n_2(ba)}}, \quad (\text{S51})$$

where  $k_2 = k_c/K_S(a)^{n_2(a)}$ . Note that with our A $\beta$ xx-A $\beta$ 42 system it has been shown that secondary nucleation of A $\beta$ xx fibrils does not occur on A $\beta$ 42 fibrils, so clusters of type- $b$  monomers almost certainly do not form on type- $a$  fibrils, and we expect  $n_2(ba) = 1$ . Indeed, the kinetics of A $\beta$ 42 aggregation inhibition by A $\beta$ xx monomers is shown in the main text (Fig. 3c) to be well-described by a model where  $n_2(ba) = 1$ , i.e. only one A $\beta$ xx monomer can bind to a given secondary nucleation site on an A $\beta$ 42 fibril. Noting that  $r_S = \alpha_{2,a}M_a(t)$ , nondimensionalization yields finally Eq. (10) in the main text.

### A. More detailed derivation

If type- $b$  monomers can compete with type- $a$  monomers for binding to secondary nucleation sites on type- $a$  fibrils, the total mass concentration of A $\beta$ 42 fibrils is:

$$M_a = M_a^f + M_a^b + \sum_{i=1}^N M_a^{ai}, \quad (\text{S52})$$

where  $M_a^f$  is the free (unbound) fibril mass concentration,  $M_a^{ai}$  is the concentration of monomeric subunits within type- $a$  fibrils bound by a cluster of  $i$  monomers of type  $a$ , and  $N$  is the maximum cluster size that can attach to a nucleation site. Finally,  $M_a^b$  is the concentration of monomeric subunits within type- $a$  fibrils bound by type- $b$  monomers. Clusters of type- $b$  monomers are neglected because under the present experimental conditions it has been shown that secondary nucleation of A $\beta$ xx fibrils does not occur on A $\beta$ 42 fibrils. This simplification would appear justified given the successful fit of our ultimate model to kinetic data of A $\beta$ 42 aggregation inhibition by A $\beta$ xx monomers (Fig. 3c). Using the previously successful [6] simplifying assumption that pre-equilibrium is achieved between bound and unbound states, we may write:

$$\frac{m_a M_a^f}{M_a^{a1}} = K_1, \quad \frac{m_a M_a^{a1}}{M_a^{a2}} = K_2, \quad \dots \quad (\text{S53})$$

where  $K_i$  is the equilibrium constant for the unbinding of a monomer from a secondary nucleation site on a type- $a$  fibril with  $i$  type- $a$  monomers bound to it. Combining these equations allows us to express the total type- $a$  fibril mass concentration as:

$$M_a = M_a^f \left( \sum_{i=0}^N m_a^i / \prod_{j=1}^i K_j + m_b / K_S(ba) \right), \quad (\text{S54})$$

where  $K_S(ba)$  is the equilibrium constant for the unbinding of type- $b$  monomers from type- $a$  fibrils. In turn,  $M_a^{ai}$  becomes:

$$M_a^{ai} = \frac{m_a^i}{\prod_{j=1}^i K_j} M_a^f \quad (\text{S55})$$

$$= \frac{m_a^i / \prod_{j=1}^i K_j}{\sum_{i=0}^N m_a^i / \prod_{j=1}^i K_j + m_b / K_S(ba)} M_a. \quad (\text{S56})$$

Considering that the full rate of generation of new type- $a$  fibrils by secondary nucleation is:

$$r_S = \sum_{i=2}^N 2k_{ci} M_a^{ai}, \quad (\text{S57})$$

where  $k_{ci}$  are conversion rate constants, this ultimately yields:

$$r_S = \frac{\sum_{i=2}^N 2k_{ci} m_a^i / \prod_{j=1}^i K_j}{\sum_{i=0}^N m_a^i / \prod_{j=1}^i K_j + m_b / K_S(ba)} M_a(t). \quad (\text{S58})$$

This expression obviously has far too many parameters to reasonably determine via data fitting, so a simplification is in order. To achieve this, we first note that cluster conversion to fibrillar structure has been shown [59] to start in a sub-cluster of defined size  $i^*$ . Thus below  $i = i^*$  we expect  $k_{ci} \simeq 0$ , whereas for  $i > i^*$  we do not expect strong variation of  $k_{ci}$  with size, i.e.  $k_{ci} \simeq k_c$ . So we can approximate the rate as <sup>3</sup>:

$$r_S \simeq \frac{2k_c \sum_{i=i^*}^N m_a^i / \prod_{j=1}^i K_j}{\sum_{i=0}^N m_a^i / \prod_{j=1}^i K_j + m_b / K_S(ba)} M_a(t). \quad (\text{S59})$$

Now, at low enough  $m_a$  the numerator and denominator sums are dominated by their first terms, i.e.  $m_a^{i^*} / \prod_{j=1}^{i^*} K_j$  and 1. At high enough  $m_a$ , by contrast, the denominator sum (and entire denominator) is dominated by the terms  $\sum_{i=i^*}^N m_a^i / \prod_{j=1}^i K_j$ , with the rate simplifying to  $k_c M_a(t)$ . At all concentrations, therefore, and identifying  $i^* = n_2(a)$ , we may approximate the rate by:

$$r_S \simeq \frac{2k_2(a)m_a(t)^{n_2(a)}M_a(t)}{1 + (m_a(t)/K_S(a))^{n_2(a)} + (m_b(0)/K_S(ba))^{n_2(ba)}}, \quad (\text{S60})$$

where  $K_S(a)$  is the geometric mean of the individual unbinding step equilibrium constants  $(\prod_{j=1}^{i^*} K_j)^{1/i^*}$ , and  $k_2 = k_c / K_S(a)^{n_2(a)}$ . The transition between low and high  $m_a$  will not match the full model Eq. (S58); however, detecting the differences would require fitting to

<sup>3</sup> Note that  $i^*$  could instead correspond to the smallest cluster to be appreciably populated at equilibrium, if there is a sharp lower cut-off in the size distribution that is stable over a wide range of monomer concentrations (as occurs for spherical micellar clusters [60]), and if this cut-off is larger than the minimum converting cluster size.

datasets with far lower experimental error than is practically achievable, exploring specifically the regime  $m_a \simeq K_S(a)$ . Non-integer  $n_2(a)$ 's may arise when two clusters contribute to the low- $m_a$  limit of the numerator. This can arise due to  $k_{c,i-1}$  being small compared to  $k_c$ , but still non-zero.

## S5. NONDIMENSIONAL RATE EQUATIONS FOR AB42-ABXX COAGGREGATION

### A. Nondimensionalization of A $\beta$ 42 fibril formation equations

Eqs. (8) can be nondimensionalized using  $\mu_a(t) = m_a(t)/m_{\text{tot},a}$ ,  $\Pi_a(t) = 2k_+(a)P_a(t)/\kappa_a$  and  $\tau_a = \kappa_a t$ , where  $\kappa_a = \sqrt{\alpha_{e,a}(m_{\text{tot},a})\alpha_{2,a}(m_{\text{tot},a})}$ , giving:

$$\frac{d\Pi_a}{d\tau_a} = 2\varepsilon_a \mu_a^{n_c(a)} + \mu_a^{n_2(a)}(1 - \mu_a) \frac{1 + 1/\mathcal{K}_S(a)^{n_2(a)} + 1/\mathcal{K}_S(ba)}{1 + \mu_a^{n_2(a)}/\mathcal{K}_S(a)^{n_2(a)} + 1/\mathcal{K}_S(ba)}, \quad (\text{S61a})$$

$$\frac{d\mu_a}{d\tau_a} = -\mu_a(\tau_a)\Pi_a(\tau_a), \quad (\text{S61b})$$

$$\varepsilon_a = \frac{\alpha_{1,a}(m_{\text{tot},a})}{2m_{\text{tot},a}\alpha_{2,a}(m_{\text{tot},a})}, \quad (\text{S61c})$$

where  $\mathcal{K}_S(a) = K_S(a)/m_{\text{tot},a}$  and  $\mathcal{K}_S(ba) = K_S(ba)/m_{\text{tot},b}$  are the dimensionless dissociation constants for types  $a$  and  $b$  monomers from type- $a$  fibrils.

### B. Nondimensionalization of A $\beta$ xx fibril formation equations

For mathematical convenience, we describe the rate  $r$  of production of A $\beta$ xx nuclei via cross-secondary nucleation in Eqs. (11) with the simplified rate law  $r = 2k_2(ba)m_a^{n_2(ba)}m_b^{n_2(bb)}$ . Saturation of the A $\beta$ 42 fibrils with respect to either type of monomer can be modelled quite accurately by setting either  $n_2(ba)$  or  $n_2(bb)$  close to zero, as appropriate. This holds so long as the initial saturation states in different experiments within the datasets are similar.

Eqs. (11) can be nondimensionalized using  $\mu_b(t) = m_b(t)/m_{\text{tot},b}$ ,  $\Pi_b(t) = 2k_+(b)P_b(t)/\kappa_b$  and  $\tau_b = \kappa_b t$  and  $\mu_b = m_b/m_{\text{tot},b}$ , where  $\kappa_b = \sqrt{\alpha_{e,b}(m_{\text{tot},b})\alpha_{2,b}(m_{\text{tot},b})}$

yielding:

$$\begin{aligned} \frac{d\Pi_b}{d\tau_b} &= 2\varepsilon_b \mu_b(\tau_b)^{n_c(b)} + 2\varepsilon_{1,ba} \mu_a(\tau_a)^{n_c(ba)} \mu_b(\tau_b)^{n_c(bb)} \\ &+ 2\varepsilon_{2,ba} \mu_a(\tau_a)^{n_2(ba)} \mu_b(\tau_b)^{n_2(bb)} (1 - \mu_a(\tau_a)) \\ &+ \frac{1 + \mathcal{K}_S(b)^{n_2(b)}}{\mu_b(\tau_b)^{n_2(b)} + \mathcal{K}_S(b)^{n_2(b)}} \mu_b(\tau_b)^{n_2(b)} (1 - \mu_b(\tau_b)), \end{aligned} \quad (\text{S62a})$$

$$\frac{d\mu_b}{d\tau_b} = -\mu_b(\tau_b)\Pi_b(\tau_b), \quad (\text{S62b})$$

$$\mu_b(0) = 1 - \delta, \quad \Pi_b(0) = p, \quad (\text{S62c})$$

where  $\mathcal{K}_S(b) = K_S(b)/m_{\text{tot},b}$  and:

$$\varepsilon_{1,ba} = \frac{\alpha_{1,ba}(m_{\text{tot},a}, m_{\text{tot},b})}{2m_{\text{tot},b}\alpha_{2,b}(m_{\text{tot},b})}, \quad (\text{S63a})$$

$$\varepsilon_{2,ba} = \frac{m_{\text{tot},a}\alpha_{2,ba}(m_{\text{tot},a}, m_{\text{tot},b})}{2m_{\text{tot},b}\alpha_{2,b}(m_{\text{tot},b})}, \quad (\text{S63b})$$

$$\varepsilon_b = \frac{\alpha_{1,b}(m_{\text{tot},b})}{2m_{\text{tot},b}\alpha_{2,b}(m_{\text{tot},b})}. \quad (\text{S63c})$$

### C. Applicability of method of asymptotic Lie symmetries

Importantly, we can identify  $\mathcal{K}_S(a)^{-1} = 0$  with parameter  $\mathbf{d}$  from the Methods; when set to zero alongside  $\varepsilon_a$ , Eqs. (S61) reduce to Eqs. (S8) with  $\varepsilon = 0$  and thus possess the same special solution, i.e. Eq. (S27) (identifying  $\tau = \tau_a$  and  $n_2 = n_2(a)$ ). Asymptotic symmetries involving  $\mathcal{K}_S(a)^{-1}$  and  $\varepsilon_a$  computed from the local perturbation series of Eq. (S61) around  $\mu_a = 1 - \delta$ ,  $\Pi_a = p_0(\delta)$  are valid globally, provided  $\varepsilon_a$  is small (as is the case in unseeded A $\beta$  kinetics, and indeed in most protein aggregation reactions hitherto studied[11]).

For large values of  $\mathcal{K}_S(a)^{-1}$ , this is because secondary nucleation does not now reduce significantly until  $\mu_a \ll 1$ . As a consequence, the  $\mu_a \rightarrow 0$  asymptotic limit is visited too late during saturating aggregation for its perturbation by the introduction of non-zero  $\mathcal{K}_S(a)^{-1}$  and  $\varepsilon$  to be important for the overall kinetics.

For small values of  $\mathcal{K}_S(a)^{-1}$  this is because  $\varepsilon_a$  and  $\mathcal{K}_S(a)^{-1}$  then drop out of the  $\mu \rightarrow 0$  kinetics at leading order, and such symmetries therefore have no effect in this regime. This may be seen as follows. Integrating Eqs. (S61) once with  $\Pi(\mu = 1) = 1$  yields  $\Pi$  as a function of  $\mu$ . Taking the limit  $\mu \rightarrow 0$  then yields  $\Pi(\infty)$ :

$$\begin{aligned} \Pi_a(\infty) &= \left( \frac{2(A+B)}{Bn_2(a)} \ln \left[ 1 + \frac{B}{A} \right] + 4 \frac{\varepsilon_a}{n_c} \right. \\ &\left. - \frac{2(A+B)}{A(1+n_2(a))} {}_2F_1 \left[ 1, 1 + \frac{1}{n_2(a)}, 2 + \frac{1}{n_2(a)}, -\frac{B}{A} \right] \right)^{1/2}, \end{aligned} \quad (\text{S64})$$

where  $A = 1 + 1/\mathcal{K}_S(ba)$ , and  $B = 1/\mathcal{K}_S(a)^{n_2(a)}$ . In the limit of small  $\mathcal{K}_S(a)^{-1}$ , and noting that the first-order

Taylor series around  $z = 0$  of  ${}_2F_1[a, b, c, z]$  is  $1 + abz/c$ , the hypergeometric becomes:

$${}_2F_1\left[1, \frac{n_2(a)+1}{n_2(a)}, \frac{2n_2(a)+1}{n_2(a)}, -\frac{B}{A}\right] \rightarrow 1 - \frac{n_2(a)+1}{2n_2(a)+1} \frac{B}{A} + O(\mathcal{K}_S(a)^{-2n_2(a)}), \quad (\text{S65})$$

and  $\Pi_a(\infty)$  reduces to:

$$\Pi_a(\infty) = \sqrt{\frac{2}{n_2(a)} - \frac{2}{n_2(a)+1}} + O(\mathcal{K}_S(a)^{-n_2(a)}, \varepsilon_a). \quad (\text{S66})$$

Thus, to leading order,  $\mu_a \rightarrow 1$  asymptotic symmetries in  $\mathcal{K}_S(a)^{-n_2(a)}, \varepsilon_a$  have no effect on the  $\mu_a \rightarrow 0$  dynamics.

Since A $\beta$ 42 aggregation is complete before A $\beta$ xx aggregation begins, the solution to the kinetics of A $\beta$ 42 aggregation in the presence of constant A $\beta$ xx monomer concentration, Eq. (13), may be substituted for  $m_a(t)$  and  $M_a(t)$  (or Eq. (S86) when A $\beta$ 42 fibril seeds are present). Once more, Eq. (S27) is a special solution to Eq. (11) with the right initial conditions when  $\{\varepsilon_b, \varepsilon_{1,ba}, \varepsilon_{2,ba}, \mathcal{K}_S(b)^{-1}\} = 0$ . Because Eqs. (S62) are also of the same form as Eqs. (S61), asymptotic symmetries around  $\mu_b = 1 - \delta$ ,  $\Pi_a = p_0(\delta)$  are again valid globally; the method of solution by asymptotic symmetries can thus again be used.

## S6. FIRST-ORDER PERTURBATION SERIES FOR AB42-ABXX COAGGREGATION

### A. Perturbation series for $\mu_a$

Pre-multiplying  $\varepsilon_a$  in Eqs. (S61) by perturbation parameter  $s$  gives:

$$\frac{d\Pi_a}{d\tau_a} = 2s\varepsilon_a\mu_a^{n_c(a)} + \mu_a^{n_2(a)}(1 - \mu_a) \frac{1 + 1/\mathcal{K}_S(a)^{n_2(a)} + 1/\mathcal{K}_S(ba)}{1 + \mu_a^{n_2(a)}/\mathcal{K}_S(a)^{n_2(a)} + 1/\mathcal{K}_S(ba)}, \quad (\text{S67a})$$

$$\frac{d\mu_a}{d\tau_a} = -\mu_a(\tau_a)\Pi_a(\tau_a), \quad (\text{S67b})$$

$$\varepsilon_a = \frac{\alpha_{1,a}(m_{\text{tot},a})}{2m_{\text{tot},a}\alpha_{2,a}(m_{\text{tot},a})}. \quad (\text{S67c})$$

Substituting in  $\mu_a = \mu_a^{(0)} + s\mu_a^{(1)} + s^2\mu_a^{(2)}$  and  $\Pi_a = \Pi_a^{(0)} + s\Pi_a^{(1)} + s^2\Pi_a^{(2)}$ , and expanding order-by-order in  $s$  for low-seed initial conditions  $\mu_a(0) = 1 - s\delta$ ,  $\Pi_a(0) = sp$ , yields the following perturbation equations at zeroth order:

$$\frac{d\Pi_a^{(0)}}{d\tau_a} = (\mu_a^{(0)})^{n_2(a)}(1 - \mu_a^{(0)}) \frac{1 + 1/\mathcal{K}_S(a)^{n_2(a)} + 1/\mathcal{K}_S(ba)}{1 + (\mu_a^{(0)})/\mathcal{K}_S(a)^{n_2(a)} + 1/\mathcal{K}_S(ba)} \quad (\text{S68a})$$

$$\frac{d\mu_a^{(0)}}{d\tau_a} = -\mu_a^{(0)}\Pi_a^{(0)}. \quad (\text{S68b})$$

As before, these are solved by  $\mu_a^{(0)} = 1$ ,  $\Pi_a^{(0)} = 0$ . At first order in  $s$ , the perturbation equations then become:

$$\frac{d\Pi_a^{(1)}}{d\tau_a} = 2\varepsilon_a - \mu_a^{(1)} \quad (\text{S69a})$$

$$\frac{d\mu_a^{(1)}}{d\tau_a} = -\Pi_a^{(1)}. \quad (\text{S69b})$$

These are solved by:

$$\mu_a^{(1)} = -\delta - \left(\varepsilon_a + \frac{\delta}{2}\right) (e^{\tau_a} + e^{-\tau_a} - 2) - \frac{p}{2}(e^{\tau_a} - e^{-\tau_a}), \quad (\text{S70a})$$

$$\Pi_a^{(1)} = \left(\varepsilon_a + \frac{\delta}{2}\right) (e^{\tau_a} - e^{-\tau_a}) + \frac{p}{2}(e^{\tau_a} + e^{-\tau_a}). \quad (\text{S70b})$$

### B. Perturbation series for $\mu_b$

The differential equations to be solved are Eqs. (S62):

$$\begin{aligned} \frac{d\Pi_b}{d\tau_b} &= 2\varepsilon_b\mu_b(\tau_b)^{n_c(b)} + 2\varepsilon_{1,ba}\mu_a(\tau_a)^{n_c(ba)}\mu_b(\tau_b)^{n_c(bb)} + 2\varepsilon_{2,ba}\mu_a(\tau_a)^{n_2(ba)}\mu_b(\tau_b)^{n_2(bb)}(1 - \mu_a(\tau_a)) \\ &\quad + \frac{1 + \mathcal{K}_S(b)^{n_2(b)}}{\mu_b(\tau_b)^{n_2(b)} + \mathcal{K}_S(b)^{n_2(b)}}\mu_b(\tau_b)^{n_2(b)}[1 - \mu_b(\tau_b)], \end{aligned} \quad (\text{S71a})$$

$$\frac{d\mu_b}{d\tau_b} = -\mu_b(\tau_b)\Pi_b(\tau_b), \quad (\text{S71b})$$

subject to initial conditions  $\mu_b(0) = 1$ ,  $\Pi_b(0) = 0$ . We pre-multiply the small terms proportional to  $\varepsilon_b$ ,  $\varepsilon_{1,ba}$  and  $\varepsilon_{2,ba}$  by perturbation indexing parameter  $s$  (to be later set to 1), as before. Substituting in  $\mu_b = 1 + s\mu_b^{(1)}$  and  $\Pi_b = s\Pi_b^{(1)}$  then gives the following equations at first order in  $s$ :

$$\frac{d\Pi_b^{(1)}}{d\tau_b} = 2\varepsilon_b + 2\varepsilon_{1,ba}\mu_a(\tau_a)^{n_c(ba)} + 2\varepsilon_{2,ba}\mu_a(\tau_a)^{n_2(ba)}(1 - \mu_a(\tau_a)) - \mu_b^{(1)}(\tau_b), \quad (\text{S72a})$$

$$\frac{d\mu_b^{(1)}}{d\tau_b} = -\Pi_b^{(1)}(\tau_b). \quad (\text{S72b})$$

In the limits  $e^{\kappa_a t} \gg 1$  and  $\delta \ll 1$ , the low-seed solution for  $\mu_a$  (Eq. (S86)) becomes:  $\mu_a \rightarrow (1 + Ae^{\kappa_a t}/c_a)^{-c_a}$ , where  $A = \varepsilon_a + \delta/2 + p/2$ . At this point, Eqs. (S72) may be solved for  $\mu_b^{(1)}$  as:

$$\begin{aligned} \mu_b^{(1)}(t) &= -\varepsilon_{1,ba} \left( e^{\kappa_b t} {}_2F_1 \left[ -\frac{\kappa_b}{\kappa_a}, c_a n_c(ba), 1 - \frac{\kappa_b}{\kappa_a}, -\frac{A}{c_a} \right] - {}_2F_1 \left[ -\frac{\kappa_b}{\kappa_a}, c_a n_c(ba), 1 - \frac{\kappa_b}{\kappa_a}, -\frac{A}{c_a} e^{\kappa_a t} \right] \right. \\ &\quad \left. + e^{-\kappa_b t} {}_2F_1 \left[ \frac{\kappa_b}{\kappa_a}, c_a n_c(ba), 1 + \frac{\kappa_b}{\kappa_a}, -\frac{A}{c_a} \right] - {}_2F_1 \left[ \frac{\kappa_b}{\kappa_a}, c_a n_c(ba), 1 + \frac{\kappa_b}{\kappa_a}, -\frac{A}{c_a} e^{\kappa_a t} \right] \right) \\ &\quad - \varepsilon_{2,ba} \left( e^{\kappa_b t} {}_2F_1 \left[ -\frac{\kappa_b}{\kappa_a}, c_a n_2(ba), 1 - \frac{\kappa_b}{\kappa_a}, -\frac{A}{c_a} \right] - e^{\kappa_b t} {}_2F_1 \left[ -\frac{\kappa_b}{\kappa_a}, c_a(1 + n_2(ba)), 1 - \frac{\kappa_b}{\kappa_a}, -\frac{A}{c_a} \right] \right. \\ &\quad \left. + e^{-\kappa_b t} {}_2F_1 \left[ \frac{\kappa_b}{\kappa_a}, c_a n_2(ba), 1 + \frac{\kappa_b}{\kappa_a}, -\frac{A}{c_a} \right] - e^{-\kappa_b t} {}_2F_1 \left[ \frac{\kappa_b}{\kappa_a}, c_a(1 + n_2(ba)), 1 + \frac{\kappa_b}{\kappa_a}, -\frac{A}{c_a} \right] \right. \\ &\quad \left. + {}_2F_1 \left[ -\frac{\kappa_b}{\kappa_a}, c_a(1 + n_2(ba)), 1 - \frac{\kappa_b}{\kappa_a}, -\frac{A}{c_a} e^{\kappa_a t} \right] - {}_2F_1 \left[ -\frac{\kappa_b}{\kappa_a}, c_a n_2(ba), 1 - \frac{\kappa_b}{\kappa_a}, -\frac{A}{c_a} e^{\kappa_a t} \right] \right. \\ &\quad \left. + {}_2F_1 \left[ \frac{\kappa_b}{\kappa_a}, c_a(1 + n_2(ba)), 1 + \frac{\kappa_b}{\kappa_a}, -\frac{A}{c_a} e^{\kappa_a t} \right] - {}_2F_1 \left[ \frac{\kappa_b}{\kappa_a}, c_a n_2(ba), 1 + \frac{\kappa_b}{\kappa_a}, -\frac{A}{c_a} e^{\kappa_a t} \right] \right) - \varepsilon_b (e^{\kappa_b t} + e^{-\kappa_b t} - 2), \end{aligned} \quad (\text{S73})$$

where  ${}_2F_1[a, b, c, z]$  is the Gaussian hypergeometric function. Since  $A/c_a \ll 1$  provided seed concentration is low, and since  $\lim_{z \rightarrow 0} {}_2F_1[a, b, c, z] = 1$ , the first four terms proportional to  $\varepsilon_{2,ba}$  cancel, and two of the hypergeometrics proportional to  $\varepsilon_{1,ba}$  vanish, simplifying Eq. (S73) to:

$$\begin{aligned} \mu_b^{(1)}(t) &= -\varepsilon_{1,ba} \left( e^{\kappa_b t} - {}_2F_1 \left[ -\frac{\kappa_b}{\kappa_a}, c_a n_c(ba), 1 - \frac{\kappa_b}{\kappa_a}, -\frac{A}{c_a} e^{\kappa_a t} \right] + e^{-\kappa_b t} - {}_2F_1 \left[ \frac{\kappa_b}{\kappa_a}, c_a n_c(ba), 1 + \frac{\kappa_b}{\kappa_a}, -\frac{A}{c_a} e^{\kappa_a t} \right] \right) \\ &\quad - \varepsilon_{2,ba} \left( {}_2F_1 \left[ -\frac{\kappa_b}{\kappa_a}, c_a(1 + n_2(ba)), 1 - \frac{\kappa_b}{\kappa_a}, -\frac{A}{c_a} e^{\kappa_a t} \right] - {}_2F_1 \left[ -\frac{\kappa_b}{\kappa_a}, c_a n_2(ba), 1 - \frac{\kappa_b}{\kappa_a}, -\frac{A}{c_a} e^{\kappa_a t} \right] \right. \\ &\quad \left. + {}_2F_1 \left[ \frac{\kappa_b}{\kappa_a}, c_a(1 + n_2(ba)), 1 + \frac{\kappa_b}{\kappa_a}, -\frac{A}{c_a} e^{\kappa_a t} \right] - {}_2F_1 \left[ \frac{\kappa_b}{\kappa_a}, c_a n_2(ba), 1 + \frac{\kappa_b}{\kappa_a}, -\frac{A}{c_a} e^{\kappa_a t} \right] \right) - \varepsilon_b (e^{\kappa_b t} + e^{-\kappa_b t} - 2), \end{aligned} \quad (\text{S74})$$

Bearing in mind the following identity:

$${}_2F_1[a, b, c, z] \equiv \frac{1}{(1-z)^a} {}_2F_1 \left[ a, c-b, c, \frac{z}{z-1} \right], \quad (\text{S75})$$

and since  $\frac{\varepsilon_a}{c_a} e^{\kappa_a t} \gg 1$  by the time the type- $b$  sigmoid is reached, the remaining hypergeometric functions can be simplified using the relations:

$${}_2F_1\left[-\frac{\kappa_b}{\kappa_a}, n_x, 1 - \frac{\kappa_b}{\kappa_a}, -\frac{A}{c_a}e^{\kappa_a t}\right] \equiv \left(1 + \frac{A}{c_a}e^{\kappa_a t}\right)^{\frac{\kappa_b}{\kappa_a}} {}_2F_1\left[-\frac{\kappa_b}{\kappa_a}, 1 - \frac{\kappa_b}{\kappa_a} - n_x, 1 - \frac{\kappa_b}{\kappa_a}, \frac{\frac{A}{c_a}e^{\kappa_a t}}{1 + \frac{A}{c_a}e^{\kappa_a t}}\right] \quad (\text{S76})$$

$$\simeq e^{\kappa_b t} \left(\frac{A}{c_a}\right)^{\kappa_b/\kappa_a} {}_2F_1\left[-\frac{\kappa_b}{\kappa_a}, 1 - \frac{\kappa_b}{\kappa_a} - n_x, 1 - \frac{\kappa_b}{\kappa_a}, 1\right] \quad (\text{S77})$$

$${}_2F_1\left[\frac{\kappa_b}{\kappa_a}, n_x, 1 + \frac{\kappa_b}{\kappa_a}, -\frac{A}{c_a}e^{\kappa_a t}\right] \equiv \left(1 + \frac{A}{c_a}e^{\kappa_a t}\right)^{-\frac{\kappa_b}{\kappa_a}} {}_2F_1\left[\frac{\kappa_b}{\kappa_a}, 1 + \frac{\kappa_b}{\kappa_a} - n_x, 1 + \frac{\kappa_b}{\kappa_a}, \frac{\frac{A}{c_a}e^{\kappa_a t}}{1 + \frac{A}{c_a}e^{\kappa_a t}}\right] \quad (\text{S78})$$

$$\simeq e^{-\kappa_b t} \left(\frac{A}{c_a}\right)^{-\kappa_b/\kappa_a} {}_2F_1\left[\frac{\kappa_b}{\kappa_a}, 1 + \frac{\kappa_b}{\kappa_a} - n_x, 1 + \frac{\kappa_b}{\kappa_a}, 1\right]. \quad (\text{S79})$$

This gives:

$$\begin{aligned} \mu_b^{(1)}(t) = & -\varepsilon_b (e^{\kappa_b t} + e^{-\kappa_b t} - 2) - \varepsilon_{1,ba} \left( e^{\kappa_b t} \left( 1 - \left(\frac{A}{c_a}\right)^{\kappa_b/\kappa_a} {}_2F_1\left[-\frac{\kappa_b}{\kappa_a}, 1 - \frac{\kappa_b}{\kappa_a} - c_a n_c(ba), 1 - \frac{\kappa_b}{\kappa_a}, 1\right] \right) \right. \\ & \left. + e^{-\kappa_b t} \left( 1 - \left(\frac{A}{c_a}\right)^{-\kappa_b/\kappa_a} {}_2F_1\left[\frac{\kappa_b}{\kappa_a}, 1 + \frac{\kappa_b}{\kappa_a} - c_a n_c(ba), 1 + \frac{\kappa_b}{\kappa_a}, 1\right] \right) \right) \\ & - \varepsilon_{2,ba} \left( e^{\kappa_b t} \left(\frac{\varepsilon_a}{c_a}\right)^{\kappa_b/\kappa_a} \sum_{i=0}^1 (-1)^{i+1} {}_2F_1\left[-\frac{\kappa_b}{\kappa_a}, 1 - \frac{\kappa_b}{\kappa_a} - c_a(n_2(ba) + i), 1 - \frac{\kappa_b}{\kappa_a}, 1\right] \right. \\ & \left. + e^{-\kappa_b t} \left(\frac{\varepsilon_a}{c_a}\right)^{-\kappa_b/\kappa_a} \sum_{i=0}^1 (-1)^{i+1} {}_2F_1\left[\frac{\kappa_b}{\kappa_a}, 1 + \frac{\kappa_b}{\kappa_a} - c_a(n_2(ba) + i), 1 + \frac{\kappa_b}{\kappa_a}, 1\right] \right), \quad (\text{S80}) \end{aligned}$$

These simplifications mean the solution no longer satisfies the initial condition  $\mu_b^{(1)}(0) = -\delta$ . We can restore this limiting behaviour by adding and subtracting constant terms and terms proportional to  $e^{-\kappa_b t}$ , yielding finally:

$$\mu_b^{(1)}(\tau_b) \simeq - \left( \varepsilon_b + \varepsilon_{1,ba} - \varepsilon_{1,ba} \left(\frac{2\varepsilon_a + \delta + p}{2c_a}\right)^{\frac{\kappa_b}{\kappa_a}} f_1 + \varepsilon_{2,ba} \left(\frac{2\varepsilon_a + \delta + p}{2c_a}\right)^{\frac{\kappa_b}{\kappa_a}} f_2 \right) (e^{\tau_b} + e^{-\tau_b} - 2), \quad (\text{S81a})$$

$$f_1 = {}_2F_1\left[-\frac{\kappa_b}{\kappa_a}, 1 - \frac{\kappa_b}{\kappa_a} - c_a n_c(ba), 1 - \frac{\kappa_b}{\kappa_a}, 1\right], \quad (\text{S81b})$$

$$f_2 = {}_2F_1\left[-\frac{\kappa_b}{\kappa_a}, 1 - \frac{\kappa_b}{\kappa_a} - c_a(1 + n_2(ba)), 1 - \frac{\kappa_b}{\kappa_a}, 1\right] - {}_2F_1\left[-\frac{\kappa_b}{\kappa_a}, 1 - \frac{\kappa_b}{\kappa_a} - c_a n_2(ba), 1 - \frac{\kappa_b}{\kappa_a}, 1\right]. \quad (\text{S81c})$$

Because the added and subtracted terms vanish in front of the leading-order terms, this does not appreciably reduce accuracy of the final expression.

## S7. SOLUTIONS BY ASYMPTOTIC LIE SYMMETRIES

As a recap, the general solution (Eq. (S46)) to protein aggregation rate equations of the form Eq. (3) is:

$$\mu = \left(1 - \frac{\mu^{(1)}(\tau)}{c_1}\right)^{-c_1} \quad (\text{S82a})$$

$$c_1 = 3 \left( 2 \frac{d \ln[\alpha_2(m)\alpha_e(m)^2]}{d \ln m} \Big|_{m=m_{\text{tot}}} - 3 \right)^{-1} = \frac{3}{2n'_2 + 1}, \text{ where} \quad (\text{S82b})$$

$$n'_2 = \frac{d \ln[\alpha_2(m)\alpha_e(m)^2]}{d \ln m} \Big|_{m=m_{\text{tot}}} - 2. \quad (\text{S82c})$$

The conditions for this solution to be valid are met by both the A $\beta$ 42 and the A $\beta$ xx rate equations (as explained in Sec. S5 C).

### A. A $\beta$ 42 fibril formation kinetics

Identifying  $m = m_a$ , the rates of elongation and secondary nucleation  $\alpha_{e,a}(m_a)$  and  $\alpha_{2,a}(m_a)$  are given by Eqs. (9)-(10) in the main text. The logarithm of their product is:

$$\ln[\alpha_{2,a}(m_a)\alpha_{e,a}(m_a)^2] = \text{const.} + \ln\left[\frac{e^{(n_2(a)+2)\ln m_a}}{1 + m_{\text{tot},b}/K_S(ba) + e^{n_2(a)\ln m_a}/K_S(a)^{n_2(a)}}\right]. \quad (\text{S83})$$

Differentiating with respect to  $\ln m_a$  gives:

$$\left.\frac{d \ln[\alpha_{2,a}(m_a)\alpha_{e,a}(m_a)^2]}{d \ln m_a}\right|_{m_a=m_{\text{tot},a}} = n_2(a) + 2 - \frac{n_2(a)(m_{\text{tot},a}/K_S(a))^{n_2(a)}}{1 + m_{\text{tot},b}/K_S(ba) + (m_{\text{tot},a}/K_S(a))^{n_2(a)}}. \quad (\text{S84})$$

So:

$$n_2'(a) = n_2(a) \frac{1 + m_{\text{tot},b}/K_S(ba)}{1 + m_{\text{tot},b}/K_S(ba) + (m_{\text{tot},a}/K_S(a))^{n_2(a)}}. \quad (\text{S85})$$

In concert with the expression for  $\mu_a^{(1)}$  derived above (Eq. (S70a)), and identifying  $\tau = \tau_a$ , we can then write down the following analytical solution to the A $\beta$ 42 rate equations:

$$\frac{M_a(t)}{m_{\text{tot},a}} = 1 - (1 - \delta) \left[ 1 + \frac{p}{2c_a} (e^{\tau_a} - e^{-\tau_a}) + \frac{2\varepsilon_a + \delta}{2c_a} (e^{\kappa_a t} + e^{-\kappa_a t} - 2) \right]^{-c_a}, \quad (\text{S86a})$$

$$c_a = \frac{3}{2n_2'(a) + 1}. \quad (\text{S86b})$$

When  $\delta = p = 0$ , this reduces to Eq. (13). We test the accuracy of this solution in Fig. S3a, finding it to be highly accurate.

### B. A $\beta$ xx fibril formation kinetics

Identifying  $m = m_b$ , the rates of elongation and secondary nucleation  $\alpha_{e,b}(m_b)$  and  $\alpha_{2,b}(m_b)$  are given by Eqs. (11) in the main text. The logarithm of their product is:

$$\ln[\alpha_{2,b}(m_b)\alpha_{e,b}(m_b)^2] = \text{const.} + \ln\left[\frac{e^{(n_2(b)+2)\ln m_b}}{1 + e^{n_2(b)\ln m_b}/K_S(b)^{n_2(b)}}\right]. \quad (\text{S87})$$

Differentiating with respect to  $\ln m_b$  gives:

$$\left.\frac{d \ln[\alpha_{2,b}(m_b)\alpha_{e,b}(m_b)^2]}{d \ln m_b}\right|_{m_b=m_{\text{tot},b}} = n_2(b) + 2 - \frac{n_2(b)(m_{\text{tot},b}/K_S(b))^{n_2(b)}}{1 + (m_{\text{tot},b}/K_S(b))^{n_2(b)}}. \quad (\text{S88})$$

So:

$$n_2'(b) = n_2(b) \frac{1}{1 + (m_{\text{tot},b}/K_S(b))^{n_2(b)}}. \quad (\text{S89})$$

Identifying  $\tau = \tau_b$  and using the derived expression Eq. (S81) for  $\mu_b^{(1)}$ , we have all the components required for Eq. (14), the analytical solution to the A $\beta$ xx rate equations. Eq. (14) also depends on constants  $\bar{f}_1$  and  $\bar{f}_2$ , whose explicit forms are not shown in the main text. We show them here instead; they are given by:

$$\hat{f}_1 = h(n_c(ba)) \quad (\text{S90a})$$

$$\hat{f}_2 = (h(n_2(ba) + 1) - h(n_2(ba))) \quad (\text{S90b})$$

$$h(x) = {}_2F_1\left[-\frac{\kappa_b}{\kappa_a}, 1 - \frac{\kappa_b}{\kappa_a} - c_a x, 1 - \frac{\kappa_b}{\kappa_a}, 1\right]. \quad (\text{S90c})$$

We test the accuracy of this solution in Fig. S3b, finding it too to be highly accurate.

## S8. SUPPORTING KINETIC DATA FITTING

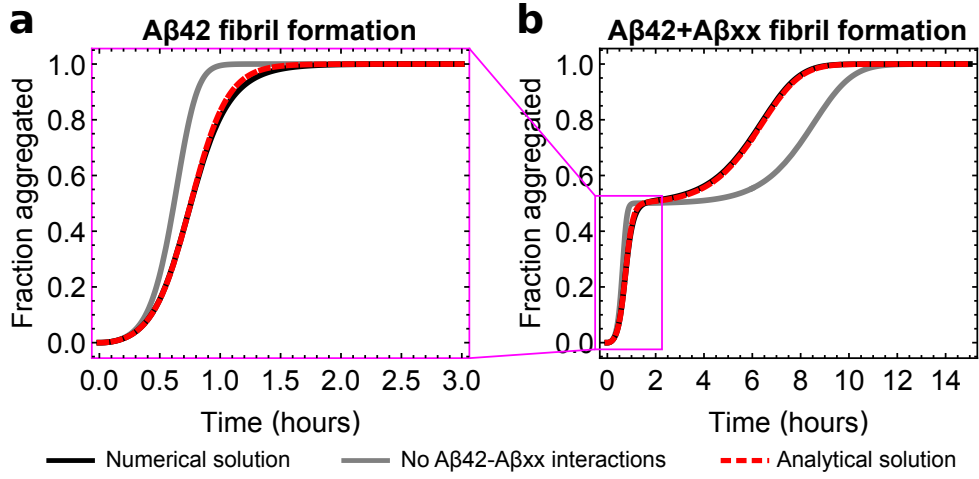


FIG. S3. Analytical solutions to the kinetics of A $\beta$ 42-A $\beta$ xx co-aggregation (red, dashed) are highly accurate, tracking the numerical solutions to the rate equations (black) almost exactly. Monomer concentrations are 4  $\mu$ M of each; rate constants are those subsequently determined by fitting experimental data for A $\beta$ 40-A $\beta$ 42 coaggregation (see Table S5). Numerical solutions in the absence of A $\beta$ 42-A $\beta$ xx interactions (gray) show a clear difference. **a**: The analytical solution to the kinetics of self-assembly of A $\beta$ 42 fibrils in the presence of A $\beta$ 40 monomers (Eqs. (13)) closely tracks the numerical solution to Eqs. (S61). **b**: Kinetics of self-assembly of all fibrils together are modelled accurately by the combined analytical solution Eq. (16), implying that A $\beta$ 40 fibrils (rate equations Eqs. (S62)) are similarly well-described by the analytical solution Eqs. (14).

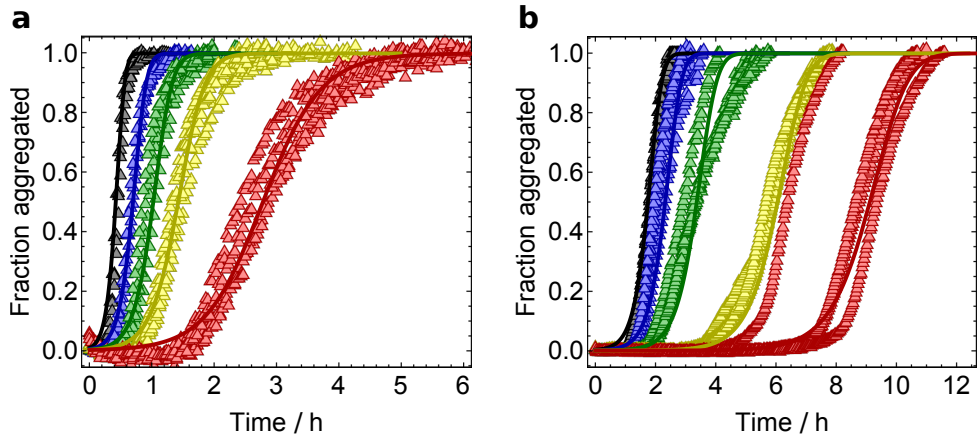


FIG. S4. Data on A $\beta$ xx and A $\beta$ 42 aggregation in isolation were collected in refs. [30, 34] alongside the coaggregation data. The catalytic secondary nucleation model, Eq. (16), yields good fits to these data. **a**: A $\beta$ 42 at pH 7.4; initial monomer concentrations are  $m(0) = 10, 5, 3, 2$  and  $1 \mu$ M. Rate parameters are  $K_S = 1.1 \mu$ M,  $n_c = n_2 = 2$ . **b**: A $\beta$ 40 at pH 7.4; initial monomer concentrations are  $m(0) = 20, 15, 10, 5$  and  $3 \mu$ M. Since  $K_S \ll 3 \mu$ M, secondary nucleation is completely saturated at these concentrations and we can only provide this bound on  $K_S$  rather than a precise value. Other rate parameters are  $n_c = 3$  and  $n_2 = 2$ .

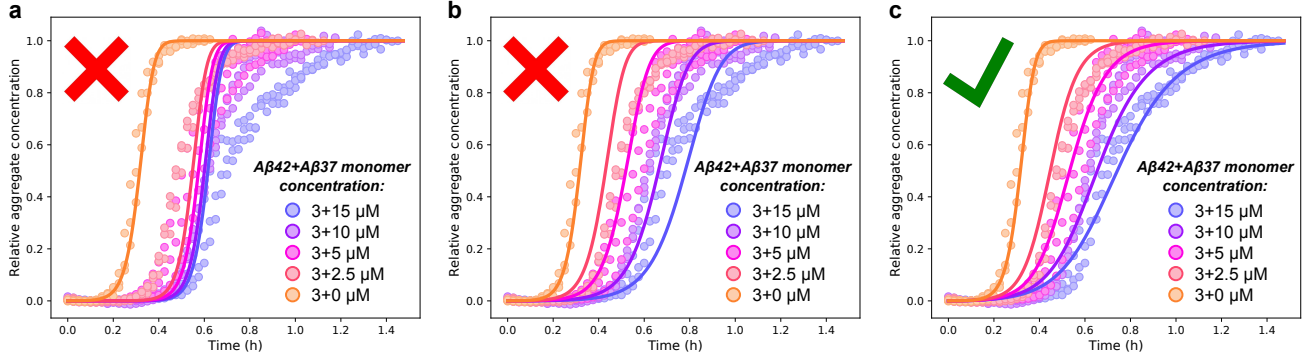


FIG. S5. Determining how A $\beta$ 42 fibril formation is inhibited by A $\beta$ 37 monomers, by global fitting of kinetic models to first sigmoid of coaggregation data for 3  $\mu$ M A $\beta$ 42 monomer with various initial A $\beta$ 37 monomer concentrations. **a**: Global misfit of model in which A $\beta$ 37 inhibits primary nucleation (Eqs. (13) with  $K_E(ba)^{-1} = K_S(ba)^{-1} = 0$ ). **b**: Global misfit to models in which A $\beta$ 37 inhibits elongation (Eqs. (13) with  $K_P(ba)^{-1} = K_S(ba)^{-1} = 0$ ). **c**: Global fit of model in which A $\beta$ 37 inhibits secondary nucleation (Eqs. (13) with  $K_E(ba)^{-1} = K_P(ba)^{-1} = 0$ ). Fitted parameter values are summarized in Tables S5-S6. The pattern of fits and misfits is identical to those for inhibition by A $\beta$ 40 and A $\beta$ 38 monomers in main text Fig. 3.

## S9. SUMMARY OF PARAMETERS

TABLE S1. Mathematical notation used throughout the paper

Parameter	Definition
$\mathbf{X}$	Symmetry generator
$s$	Perturbation indexing parameter
$x_a, x(a)$	Parameter $x$ pertaining to faster-aggregating species $a$
$x_b, x(b)$	Parameter $x$ pertaining to slower-aggregating species $b$
$m_{\text{tot}}$	Total monomer concentration
$\mu(\tau) = m(\tau)/m_{\text{tot}}$	Nondimensionalized monomer concentration
$\Pi(\tau) = 2k_+P(\tau)/\kappa$	Nondimensionalized fibril concentration
$\tau = \kappa t$	Nondimensionalized time
$\alpha_1(m)$	Primary nucleation rate
$\alpha_2(m)$	Secondary nucleation rate
$\alpha_e(m)$	Elongation rate
$\kappa = \sqrt{\alpha_e(m_{\text{tot}})\alpha_2(m_{\text{tot}})}$	Rate of proliferation of fibrils by secondary processes
$\varepsilon = \alpha_1(m_{\text{tot}})/2m_{\text{tot}}\alpha_2(m_{\text{tot}})$	Rate of secondary vs primary nucleation
$1 - \delta$	Initial dimensionless monomer concentration
$p$	Initial dimensionless fibril concentration
$k_n$	1 $^\circ$ nucleation rate constant
$k_2$	2 $^\circ$ nucleation rate constant
$k_+$	Elongation rate constant
$n_c$	1 $^\circ$ nucleation reaction order
$n_2$	2 $^\circ$ nucleation reaction order
$K_S = K_S/m_{\text{tot}}$	Nondimensionalized dissociation constant
$K_S$	Dissociation constant for monomers from fibril surfaces

In all subsequent tables, an asterisk “\*” means “chosen to be arbitrarily small”.

TABLE S2. Parameter values for A $\beta$ 42 + A $\beta$ 40 aggregation in Fig. 3

Parameter	Values (units of $\mu\text{M}$ , h)	
	A $\beta$ 42	A $\beta$ 40
$k_+k_2$	7.6	
$k_+k_n$	0.021	
$n_2$	2	
$n_c$	2	
$K_S$	1.1	
$K_S(ba)$	0.39	

TABLE S3. Parameter values for Fig. 4b

Parameter	Values (units of $\mu\text{M}$ , h)	
	A $\beta$ 42	A $\beta$ 40
$k_+k_2$	17.2	48.8
$k_+k_n$	0.012	$8.5 \times 10^{-12*}$
$n_2$	2	2
$n_c$	2	3
$K_S$	1.1	0.081
$n_2(ba)$		1
$n_2(bb)$		1
$k_2(ba)$	$1.9 \times 10^{-4}$	
$K_S(ba)$	0.39	

TABLE S4. Parameter values for Fig. 4d

Parameter	Values (units of $\mu\text{M}$ , h)	
	A $\beta$ 42	A $\beta$ 40
$k_+k_2$	19.2	71.0
$k_+k_n$	0.025	$8.5 \times 10^{-12*}$
$n_2$	2	2
$n_c$	2	3
$K_S$	1.1	0.081
$n_2(ba)$		1
$n_2(bb)$		1
$k_2(ba)$	$1.3 \times 10^{-2}$	
$K_S(ba)$	0.39	

TABLE S5. Parameter values for Fig. 5b

Parameter	Values (units of $\mu\text{M}$ , h)	
	A $\beta$ 42	A $\beta$ 40
$k_+k_2$	20	9.2
$k_+k_n$	0.0097	$8.5 \times 10^{-12*}$
$n_2$	2	2
$n_c$	2	3
$K_S$	1.1	0.081
$n_2(ba)$		2.3
$n_2(bb)$		0.0
$k_2(ba)$		$3.7 \times 10^{-3}$
$K_S(ba)$		0.39

TABLE S6. Parameter values for Fig. 5c and for A $\beta$ 42 + A $\beta$ 38 aggregation in Fig. 3

Parameter	Values (units of $\mu\text{M}$ , h)	
	A $\beta$ 42	A $\beta$ 38
$k_+k_2$	19.1	50
$k_+k_n$	0.079	$10^{-16*}$
$n_2$	2	2
$n_c$	0.01	3
$K_S$	1.1	0.099
$n_2(ba)$		0.14
$n_2(bb)$		1.5
$k_2(ba)$		$1.2 \times 10^{-4}$
$K_S(ba)$		1.6

TABLE S7. Parameter values for Fig. S5

Parameter	Values (units of $\mu\text{M}$ , h)
	A $\beta$ 42
$k_+k_2$	110
$k_+k_n$	0.132
$n_2$	2
$n_c$	0
$K_S$	1.1
$K_S(ba)$	0.22